Journal of Organometallic Chemistry 892 (2019) 51–65

Contents lists available at ScienceDirect

Journal of Organometallic Chemistry

journal homepage: www.elsevier.com/locate/jorganchem

Ruthenium-cymene containing pyridine-derived aldiimine ligands: Synthesis, characterization and application in the transfer hydrogenation of aryl ketones and kinetics studies

Thiago S. Ramos [a], Diego M. Luz [a], Rebecca D. Nascimento [a], Andressa K. Silva [b], Luciano M. Lião [b], Victor M. Miranda [c], Victor M. Deflon [c], Márcio P. de Araujo [d], Leonardo T. Ueno [e], Francisco B.C. Machado [e], Luís R. Dinelli [a], André L. Bogado [a, *]

[a] Departamento de Química, Instituto de Ciências Exatas e Naturais do Pontal, Universidade Federal de Uberlândia, Rua vinte, 1600, CEP 38304-402, Ituiutaba, MG, Brazil
[b] Instituto de Química, Universidade Federal de Goiás, Avenida Esperança, s/n, Campus Samambaia, CEP 74690-900, Goiânia, GO, Brazil
[c] Instituto de Química de São Carlos, Universidade de São Paulo, CP 780, 13560-590 São Carlos, SP, Brazil
[d] Departamento de Química, Universidade Federal do Paraná, Centro Politécnico, CP 19081, Curitiba, PR, Brazil
[e] Departamento de Química, Instituto Tecnológico de Aeronáutica, Comando-Geral de Tecnologia Aeroespacial, São José dos Campos, São Paulo 12228-900, Brazil

ARTICLE INFO

Article history:
Received 28 February 2019
Received in revised form
18 April 2019
Accepted 23 April 2019
Available online 25 April 2019

Keywords:
Half-sandwich complexes
Organometallic ruthenium complexes
Schiff base
DFT
Transfer hydrogenation
Catalysis

ABSTRACT

Five electron-rich N–N′–pyridylimine ligands, which form five-membered chelate ring when coordinate to a metal center, have been synthesized by the easily accessible condensation between 2-pyridinecarboxyaldhehyde and the corresponding substituted aniline in diethyl ether solution, in the presence of catalytic amount of *p*-toluenesulfonic acid. The reaction of N–N′–pyridylimine ligands with $[RuCl_2(p\text{-cym})]_2$ **(1)** in the presence of excess of KPF_6 led to the formation of mononuclear adducts with general formula $[RuCl(p\text{-cym})(N{-}N')]PF_6$, where N–N′ = N-phenyl-1-(pyridin-2-yl)methanimine (Amp) **(2)**, N-(4-chlorophenyl)-1-(pyridin-2-yl)methanimine (Clmp) **(3)**, N-(4-methylphenyl)-1-(pyridin-2-yl) methanimine (Memp) **(4)**, N-(4-tert-butylphenyl)-1-(pyridin-2-yl)methanimine (Tbump) **(5)**, N-(2,6-diethylphenyl)-1-(pyridin-2-yl)methanimine (Diemp) and N-[2,6-bis(propan-2-yl)phenyl]-1-(pyridin-2-yl)methanimine (Diipmp) **(7)**. Additionally, the reaction of 2-acetylbenzenolate (O–O′) with **(1)** produces a less bulky neutral congener $[RuCl(p\text{-cym})(O{-}O')]$ **(8)**. All complexes were isolated and fully characterized by molar conductivity, elemental analysis, cyclic voltammetry and spectroscopic methods, including single crystal X-ray diffraction of **(4)**, **(7)** and **(8)**. The structures **(2)**–**(7)** were also optimized with the Density Functional Theory (DFT) and theoretical absorption spectra were obtained with TD-DFT formalism. The complexes **(2)**–**(8)** were applied as pre-catalyst in the transfer hydrogenation of the acetophenone and 4-methylacetophenone, showing good catalytic activity, with productivity up to 90%, and TOF up to 302 h^{-1} within 3 h of reaction; except for **(8),** which has no activity for the catalytic reduction performed in this work. A kinetic investigation using **(3)** and **(7)** as pre-catalysts showed that the time dependence for the production of 1-phenylethanol has a sigmoidal shape, with an induction time of 20 min. The catalytic activity of **(3)** is more sensitive to the temperature variation and its rate constant (k) increases faster than for **(7)**. An Arrhenius plot reveals a smaller activation barrier (E_a) for the rate-determining step for **(7)** than for **(3)**, $E_a = 14.75$ and 49.38 kJ mol^{-1}, respectively. The $\Delta S^{\neq}$ values obtained from an Eyring plot suggest an associative mechanism in the transition state of the catalytic reactions.

1. Introduction

Ruthenium complexes containing phosphine and diphosphine ligands are in general efficient catalysts in homogeneous

* Corresponding author.
E-mail address: bogado@ufu.br (A.L. Bogado).

https://doi.org/10.1016/j.jorganchem.2019.04.022
0022-328X/

hydrogenation of apolar double bonds or transfer hydrogenation of polar double bonds [1–3]. The use of P-donor groups coordinated to the metal center is almost mandatory in this field, owing to the structure of aromatic phosphines and diphosphines, which may provide strong back-bonding with the metal center, stabilizing lower oxidation states of the ruthenium center [4]. Associated to that, the most important mechanism for H_2-hydrogenation of imines and ketones was proposed by Noyori [5,6] (Nobel Prize laureate in 2001), using diamines as a key ligand and coined the term "metal-ligand bifunctional catalysis" to refer to the catalytic systems utilizing the outer-sphere hydrogenation ligand-assisted mechanism. These findings have provided a favorable perspective to explore the synthesis and application of new mixed diamine/diphosphine [7,8] and diimine/diphosphine [8–11] containing ruthenium complexes as alternative pre-catalysts for the reduction of aryl ketones.

Outside the "Ru(P)$_2$" or "Ru(P–P)" core, it is possible to find the use of "Ru-arene" moiety with several ancillary ligands as a new highway to reach active pre-catalysts for transfer hydrogenation reactions of ketones. Keeping this in mind, attention should be pointed out to the increasing use of the following ancillary ligands associated to ruthenium-arene core: amide/diamine [12], thioamides [13], sulfonamide fragment [14], N-heterocyclic carbenes [15–18], imidazolin-2-imine [19] and molten salts-based phosphine [20].

In this regard, the use of Schiff base obtained from the condensation between 2-piridinecarboxyaldhehyde and the substituted anilines appears as an accessible source of N–N′–pyridylimine ligands, which are interesting electron-rich chelating ligands to stabilize a metal center. In this context, it is worth to mention the work described by Friedrich and co-workers, in which described the synthesis of half-sandwich complexes of platinum metals group containing N–N′ donor Schiff bases and the studies of such complexes in biological assays [21,22], oxidation of olefins [23,24] and alcohols [25], and transfer hydrogenation of ketones [26–29].

In order to contribute to this discussion, in this work we present the syntheses, characterization, electrochemistry behavior and kinetic discussions of the transfer hydrogenation of acetophenone and 4-methylacetophenone of six half-sandwich ruthenium complexes with general formula [RuCl(*p*-cym)(N–N′)]PF_6 {where N–N′ = N-phenyl-1-(pyridin-2-yl)methanimine (Amp) **(2)**, N-(4-chlorophenyl)-1-(pyridin-2-yl)methanimine (Clmp) **(3)**, N-(4-methylphenyl)-1-(pyridin-2-yl)methanimine (Memp) **(4)**, N-(4-tert-butylphenyl)-1-(pyridin-2-yl)methanimine (Tbump) **(5)**, N-(2,6-diethylphenyl)-1-(pyridin-2-yl)methanimine (Diemp) and N-[2,6-bis(propan-2-yl)phenyl]-1-(pyridin-2-yl)methanimine (Di*i*pmp) **(7)**. Additionally, due to the lack of activity of the complexes to reduce the 2-hydroxyacetophenone (HAP) to the corresponding alcohol, we performed the reaction of the deprotonated form of HAP (2-acetylbenzenolate, O–O′) with **(1)** and the complex [RuCl(*p*-cym)(O–O′)] **(8)** was isolated and characterized. Suitable single-crystals of **(4)**, **(7)** and **(8)** were grown in organic solvents and their molecular structures were determined by X-ray diffraction. Electronic spectroscopy data and their analyses were supported and interpreted using DFT and TD-DFT calculations.

2. Experimental section

2.1. Materials and methods

All reactions were carried out under argon atmosphere using standard Schlenk techniques. Solvents were purified by standard methods [30] and all chemicals used were of reagent grade or comparable purity, which were supplied and used as received from Sigma/Aldrich: $RuCl_3.xH_2O$, 2-pyridinecarboxyaldhehyde, aniline, 4-chloroaniline, 4-methylaniline, 4-*tert*-buthylaniline, 2,6-diethylaniline, 2,6-di*iso*propylaniline, hexadecane, acetophenone, 4-methylacetophenone, 4-aminoacetophenone, 4-nitroacetophenone and 2-hidroxyacetophenone.

2.2. Instrumentation

Elemental analyses were performed with a Thermo Scientific CHNS–O FLASH 2000 micro analyzer, coupled with an ultra-microbalance Mettler Toledo Model XP6.

All NMR experiments were recorded on a Bruker Avance III 500 spectrometer operated at 11.75 T; ^{1}H was observed at 500.13 MHz, using a broadband observe probehead (BBO) at 25°C, in $CDCl_3$ solution. TMS was used for internal reference for ^{1}H and the signals were labeled as *s* = singlet, *brs* = broad singlet, *brd* = broad doublet, *brt* = broad triplet, *d* = doublet, *dd* = double doublet, *ddd* = double double doublet, *dsept* = double septet, *t* = triplet, *td* = triple doublet, *tt* = triple triplet, *q* = quartet, *sept* = septet, *m* = multiplet.

FTIR spectra were recorded in an ATR apparatus with diamond cell support or conventional KBr cell of 0.2 mm length with a Jasco FTIR 4000 spectrometer in the 4000–400 cm^{-1} range.

UV/Vis were recorded on a Shimadzu spectrophotometer, model UV-1800, coupled with a thermoelectrically temperature controlled cell TCC-100 (at 25.0 ± 0.1 °C), using a quartz cell (1 cm), between 200 and 800 nm.

Electrochemical data were obtained using a potentiostat/galvanostat μ-autolab type III. Solutions of the complexes (10^{-3} mol L^{-1}) were prepared in acetonitrile using 0.1 mol L^{-1} tetrabutylammonium hexafluorophosphate (TBAH) as the supporting electrolyte. Measurements were made with a three-electrode configuration cell using a glassy carbon and platinum disc (⌀ 2 mm) as working electrode and auxiliary electrode, respectively. Ag/AgCl, 0.10 mol L^{-1} TBAH in acetonitrile was used as pseudo – reference electrode. Under the conditions used, E_{pa} for the one-electron oxidation of [Fe(η^5-C_5H_5)$_2$], added to the test solutions as a standard, is +0.43 V.

Molar conductivity of solutions of the half-sandwich ruthenium complexes (10^{-3} mol L^{-1} in CH_2Cl_2 or CH_3CN) was measured with a Mettler Toledo conductivity meter model FE30, using a Pt electrode from Mettler Toledo model inLab 710 (cell constant = 0.55 cm) with sensor temperature coupled.

The catalytic experiments were analyzed by gas chromatography with a Thermo Scientific Focus Gas Chromatograph equipped with an FID detector. An LM-120 column (polyethyleneglycol) (25 m long, 0.25 mm i.d., 0.25 μm film thickness) was used for the characterization of the catalytic products and N_2 was the carrier gas (1.0 mL min^{-1}). The temperature was programed to range from 170 °C (2 min) to 200 °C at a heating rate of 10 °C min^{-1}.

2.3. Syntheses of N–N′–pyridylimine ligands

2.3.1. General procedure

All N–N′–pyridylimine ligands were synthesized by condensation between 2-pyridinecarboxyaldhehyde (10 mmol) and the corresponding substituted aniline (10 mmol) in diethyl ether solution (30 mL), in the presence of *p*-toluenesulfonic acid (1 mmol) [31]. The resulting beige solution was stirred for 12 h at 27 °C and during this period a yellow suspension was formed. The suspension was filtered off and crystalline solid were washed with cold diethyl ether. In the case of Amp and Tbump a crude oil was obtained after solvent evaporation under reduced pressure. The ^{1}H and ^{13}C NMR listing follow the numbering described in the general structure,

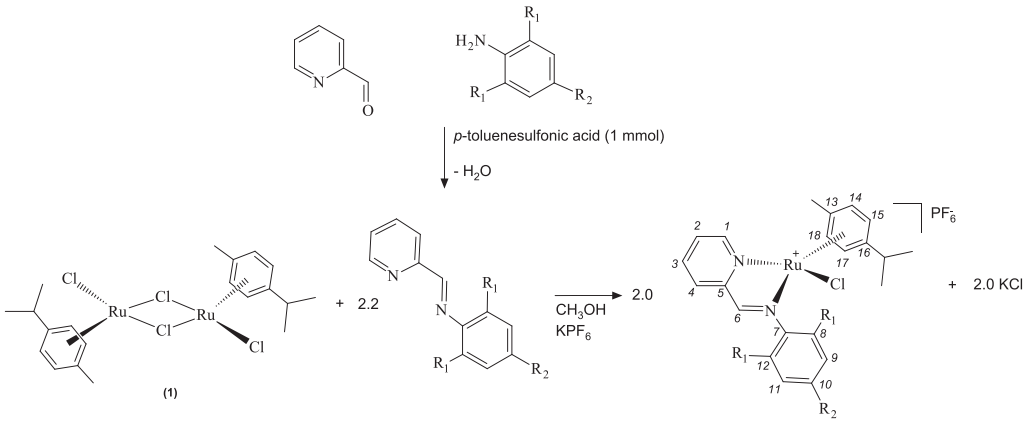

Complex	R_1	R_2
(2)	H	H
(3)	H	Cl
(4)	H	CH_3
(5)	H	*t*-But
(6)	Et	H
(7)	*i*Pr	H

Scheme 1. Synthetic route, general structure and numbering of the half-sandwich ruthenium (II) complexes [42].

which is illustrated in Scheme 1.

2.3.1.1. N-phenyl-1-(pyridin-2-yl)methanimine (Amp). Reddish oil. Yield 80–85% (1.72 g). *Anal.* calc. for $C_{12}H_{10}N_2$ (%) (exp.): C 79.09 (79.10), H 5.53 (5.61), N 15.37 (15.03). ^{1}H NMR (CD_2Cl_2 500.13 MHz) ppm: 8.50 (*dd*, $J = 4.8$, 0.9 Hz, H-1); 8.45 (*s*, H-6); 8.04 (*dd*, $J = 8.0$, 0.9 Hz, H-4); 7.60 (*ddd*, $J = 8.0$, 7.4, 0.9 Hz, H-3); 7.24 (*tt*, $J = 7.7$, 1.2 Hz, H-10); 7.15 (*ddd*, $J = 7.4$, 4.8, 0.9 Hz, H-2); 7.13 (*dd*, $J = 7.7$, 1.2 Hz, H-8/H-12); 7.10 (*td*, $J = 7.7$, 1.5 Hz, H-9/H-11). ^{13}C NMR (CD_2Cl_2 125.75 MHz) ppm: 161.47 (C-6); 155.25 (C-5); 151.61 (C-1); 150.20 (C-7); 137.19 (C-3); 129.82 (C-9/C-11); 127.24 (C-10); 125.78 (C-12); 122.00 (C-4); 121.64 (C-8/C-12). IV (KBr, cm^{-1}): 1633 ($\nu_{C=N}$ imine), 1568 ($\nu_{C=N}$ pyridine).

2.3.1.2. N-(4-chlorophenyl)-1-(pyridin-2-yl)methanimine (Clmp). Yellow powder. Yield 80–85% (1.85 g). *Anal.* calc. for $C_{12}H_9ClN_2$ (%) (exp.): C 66.52 (66.36) %, H 4.18 (3.95) %, N 12.92 (12.93) %. ^{1}H NMR (CD_3OD, 500,13 MHZ) ppm: 8.53 (*dd*, $J = 4.9$, 1.8 Hz, H-1); 8.43 (*s*, H-6); 7.80 (*td*, $J = 7.7$, 1.6 Hz, H-4); 7.74 (*td*, $J = 7.7$, 1.8 Hz, H-3); 7.25 (*dd*, $J = 4.9$, 1.6 Hz, H-2); 7.00–6.96 (*m*, H-9/H-11); 6.71–6.67 (*m*, H-8/H-12). ^{13}C NMR (CH_3OD 125.75 MHz) ppm: 160.84 (C-6); 157.75 (C-5); 149.72 (C-1); 148.90 (C-7); 138.07 (C-3); 129.61 (C-10); 129.61 (C-9/C-11); 126.24 (C-2); 122.33 (C-4); 115.55 (C-8/C-12). IV (KBr, cm^{-1}): 1626 ($\nu_{C=N}$ pyridine), 1565($\nu_{C=N}$ imine).

2.3.1.3. N-(4-methylphenyl)-1-(pyridin-2-yl)methanimine (Memp). Yellow crystals. Yield 80–85% (1.83 g). *Anal.* calc. for $C_{13}H_{12}N_2$ (%) (exp.): C 79.56 (79.40), H 6.16 (6.10), N 14.27 (14.35). ^{1}H NMR (CD_3OD 500.13 MHz) ppm: 8.46 (*dd*, $J = 4.9$, 1.6 Hz, H-1); 8.39 (*s*, H-6); 7.97 (*dd*, $J = 7.9$, 1.1 Hz, H-4); 7.71 (*ddd*, $J = 7.9$, 7.6, 1.6 Hz, H-3); 7.29 (*ddd*, $J = 7.6$, 4.9, 1.1 Hz, H-2); 7.03 (*brs*, H-8/H-9/H-11/H-12); 2.16 (*s*, CH_3-10). ^{13}C NMR (CD_3OD 125.75 MHz) ppm: 159.52 (C-6); 154.49 (C-5); 149.64 (C-1); 148.41 (C-7); 137.81 (C-10); 137.46 (C-3); 129.82 (C-9/C-11); 125.91 (C-2); 122.35 (C-4); 121.32 (C-8/C-12); 20.32 ($\underline{C}H_3$-10). IV (KBr, cm^{-1}): 1627 ($\nu_{C=N}$ imine), 1565 ($\nu_{C=N}$ pyridine).

2.3.1.4. N-(4-tert-butylphenyl)-1-(pyridin-2-yl)methanimine (Tbump). Reddish oil. Yield 70–80% (1.44 g). *Anal.* calc. for $C_{16}H_{18}N_2$ (%) (exp.): C 80.63 (80.15), H 7.61 (7.62), N 11.75 (11.99). ^{1}H NMR (CD_2Cl_2 500.13 MHz) ppm: 8.53 (*dd*, $J = 4.9$, 1.6 Hz, H-1); 8.49 (*s*, H-6); 8.07 (*dd*, $J = 7.8$, 1.1 Hz, H-4); 7.64 (*ddd*, $J = 7.8$, 7.5, 1.6 Hz, H-3); 7.32 (*brd*, $J = 8.5$ Hz, H-8/H-12); 7.19 (*ddd*, $J = 7.5$, 4.9, 1.1 Hz, H-2); 7.13 (*brd*, $J = 8.5$ Hz, H-9/H-11); 1.21 (*s*, ^{t}Bu-10). ^{13}C NMR (CD_2Cl_2 125.75 MHz) ppm: 160.67 (C-6); 155.57 (C-5); 150.58 (C-1); 150.19 (C-7); 148.95 (C-10); 137.03 (C-3); 126.71 (C-9/C-11); 125.51 (C-2); 121.87 (C-4); 121.38 (C-8/C-12); 35.05 (^{t}Bu $\underline{C}(CH_3)_3$); 31.79 (^{t}Bu $C(\underline{C}H_3)_3$). IV (KBr, cm^{-1}): 1627 ($\nu_{C=N}$ imine), 1566 ($\nu_{C=N}$ pyridine).

2.3.1.5. N-(2,6-diethylphenyl)-1-(pyridin-2-yl)methanimine (Diemp). Yellow powder. Yield 80–85% (1.89 g). *Anal.* calc. for $C_{16}H_{18}N_2$ (%) (exp.): C 80.63 (80.42), H 7.61 (7.62), N 11.75 (11.99). ^{1}H NMR (CD_2Cl_2 500.13 MHz) ppm: 8.58 (*dd*, $J = 4.8$, 1.6 Hz, H-1); 8.21 (*s*, H-6); 8.16 (*dd*, $J = 7.9$, 1.3 Hz, H-4); 7.72 (*ddd*, $J = 7.9$, 7.5, 1.6 Hz, H-3); 7.28 (*ddd*, $J = 7.5$, 4.8, 1.3 Hz, H-2); 6.99 (*d*, $J = 8.5$ Hz, H-9 or H-11); 6.99 (*d*, $J = 6.7$ Hz, H-9 or H-11); 6.92 (*dd*, $J = 8.5$, 6.7 Hz, H-10); 2.39 (*q*, $J = 7.5$ Hz, CH_2-8/CH_2-12); 1.02 (*t*, $J = 7.5$ Hz, CH_3-8/CH_3-12). ^{13}C NMR (CD_2Cl_2 125.75 MHz) ppm: 164.04 (C-6); 155.16 (C-5); 150.44 (C-1); 150.22 (C-7); 137.20 (C-3); 133.45 (C-8/C-12); 126.90 (C-9/C-11); 125.91 (C-10); 124.79 (C-2); 121.55 (C-4); 23.82 (Diemp $\underline{C}H_2CH_3$); 15.06 (Diemp $CH_2\underline{C}H_3$). IV (KBr, cm^{-1}): 1642 ($\nu_{C=N}$ imine), 1565 ($\nu_{C=N}$ pyridine).

2.3.1.6. N-[2,6-bis(propan-2-yl)phenyl]-1-(pyridin-2-yl)methanimine (Diipmp). Yellow crystals. Yield 90–95% (1.98 g). *Anal.* calc. for $C_{18}H_{22}N_2$ (%) (exp.): C 81.77 (80.28), H 7.62 (8.09), N 10.60 (10.88). ^{1}H NMR ($CDCl_3$ 500.13 MHz) ppm: 8.73 (*dd*, $J = 4.9$, 1.6 Hz,

H-1); 8.31 (*s*, H-6); 8.26 (*dd*, $J = 7.9$, 1.2 Hz, H-4); 7.85 (*ddd*, $J = 7.9$, 7.6, 1.6 Hz, H-3); 7.41 (*ddd*, $J = 7.6$, 4.9, 1.2 Hz, H-2); 7.17 (*d*, $J = 8.7$ Hz, H-9 or H-11); 7.17 (*d*, $J = 6.6$ Hz, H-9 or H-11); 7.12 (*dd*, $J = 8.7$, 6.1 Hz, H-10); 2.97 (*sept*, $J = 6.9$ Hz, C<u>H</u>$(CH_3)_2$-8/C<u>H</u>$(CH_3)_2$-12); 1.18 (*d*, $J = 6.9$ Hz, CH(C<u>H</u>$_3)_2$-8/CH(C<u>H</u>$_3)_2$-12). ^{13}C NMR ($CDCl_3$ 125.75 MHz) ppm: 162.97 (C-6); 154.41 (C-5); 149.70 (C-1); 148.40 (C-7); 137.26 (C-3); 136.74 (C-8/C-12); 125.29 (C-10); 124.47 (C-2); 123.12 (C-9/C-11); 121.33 (C-4); 27.98 (Di*ip*mp <u>C</u>$(CH_3)_2$); 23.44 (Di*ip*mp C(<u>C</u>$H_3)_2$). IV (KBr, cm^{-1}): 1633 ($\nu_{C=N}$ imine), 1568 ($\nu_{C=N}$ pyridine).

2.3.2. Syntheses of half-sandwich ruthenium (II) complexes

The general synthetic route used to synthesize the half-sandwich ruthenium (II) complexes with general formula [RuCl(*p*-cym)(N–N′)](PF_6) is described as follows:

Under an inert atmosphere of argon, [RuCl(μ-Cl)(*p*-cym)]$_2$ (0.1 g; 0.16 mmol) was dissolved in methanol (20 mL) in a Schlenk tube (100 mL) and the appropriate N–N′-pyridylimine ligand (0.35 mmol) and KPF_6 (0.066 g; 0.35 mmol) were added after total dissolution of the ruthenium precursor. The resulting red-brownish solution was kept at 27 °C and magnetically stirred for 18 h. During this period, the color changes and a yellow solution was obtained. Then, the solvent was removed under reduced pressure and the solid residue was dissolved in CH_2Cl_2 (3.0 mL), passed through a celite pad in order to remove KCl. The filtered was collected in a Schlenk flask (100 mL) and addition of diethyl ether (10 mL) yielded a yellow solid. The solid was separated by filtration, washed with diethyl ether (3 × 5 mL) and dried under reduced pressure.

The synthesis and structural characterization of **(3)** [23] and **(7)** [25] were reported previously by Friedrich and co-workers, thus, only unpublished results will be discussed here.

The ^{1}H and ^{13}C NMR listing follow the numbering described in the general structure, which is illustrated in Scheme 1.

[RuCl(*p*-cym)(Amp)]PF_6 (2)

Brown powder, yield 85–95% (0.093 g). *Anal.* calc. for $C_{22}H_{24}ClF_6N_2PRu$ (%) (exp.): C 44.19 (44.56), H 4.05 (4.35), N 4.69 (4.48). ^{1}H NMR (CD_2Cl_2 500.13 MHz) ppm: 9.24 (*brd*, $J = 5.6$ Hz, H-1); 7.69 (*dd*, $J = 5.6$, 2.6 Hz, H-2); 8.09–8.01 (*m*, H-3/H-4); 8.37 (*s*, H-6); 7.68–7.63 (*m*, H-8/H-12); 7.55–7.46 (*m*, H-9/H-10/H-11); 5.65 (*d*, $J = 6.2$ Hz, *p*-cym); 5.38 (*d*, $J = 6.2$ Hz, *p*-cym); 5.32 (*d*, $J = 6.2$ Hz, *p*-cym); 5.27 (*d*, $J = 6.2$ Hz, *p*-cym); 2.54 (*dsept*, $J = 6.9$, 7.0 Hz, C<u>H</u>$(CH_3)_2$-16); 2.14 (*s*, CH_3-13); 1.03 (*d*, $J = 7.0$ Hz, CH(C<u>H</u>$_3)_2$-16); 1.01 (*d*, $J = 6.9$ Hz, CH(C<u>H</u>$_3)_2$-16). ^{13}C NMR (CD_2Cl_2 125.75 MHz) ppm: 166.16 (C-6); 156.33 (C-5); 154.84 (C-1); 152.69 (C-7); 140.30 (C-3); 130.98 (C-10); 130.56 (C-2); 130.45 (C-9/C-11); 129.91 (C-4); 122.73 (C-8/C-12); 107.71, 104.70, 87.4, 86.6, 86.5 and 85.9 (C-13 to C-18 *p*-Cym); 32.00 (<u>C</u>H$(CH_3)_2$-16); 22.47 and 22.28 (CH(<u>C</u>$H_3)_2$-13/16); 19.20 (*p*-Cym <u>C</u>H_3). IV (KBr, cm^{-1}): 1618 ($\nu_{C=N}$ imine), 1559 ($\nu_{C=N}$ pyridine). UV/Vis (CH_3CN, 5×10^{-5} mol L^{-1}) λ/nm (log ε, L mol^{-1} cm^{-1}): 310 (3.94); 422 (3.52). CV (CH_3CN/HTBA 0.1 mol L^{-1}): $E_{ox} = 1.18$ V, $E_{red} = 1.13$ V, $E½ = 1.15$ V. Molar conductivity in CH_3CN (or CH_2Cl_2) (1.0×10^{-3} mol L^{-1}) Λm (ohm^{-1} cm^2 mol^{-1}): 73.15 (11.93).

[RuCl(*p*-cym)(Clmp)]PF_6 (3)

Yellow powder, yield 95% (0.098 g). *Anal.* calc. for $C_{22}H_{23}Cl_2F_6N_2PRu$ (%) (exp.): C 41.79 (42.12), H 3.67 (3.88), N4.43 (4.53). ^{1}H NMR (CD_2Cl_2 500.13 MHz) ppm: 9.22 (*brd*, $J = 5.5$ Hz, H-1); 7.69 (*dd*, $J = 5.5$, 2.6 Hz, H-2); 8.08–8.01 (*m*, H-3/H-4); 8.38 (*s*, H-6); 7.66 (*d*, $J = 8.5$ Hz, H-8/H-12); 7.48 (*d*, $J = 8.5$ Hz, H-9/H-11); 5.63 (*d*, $J = 6.2$ Hz, *p*-cym); 5.39 (*d*, $J = 6.2$ Hz, *p*-cym); 5.35 (*d*, $J = 6.1$ Hz, *p*-cym); 5.27 (*d*, $J = 6.1$ Hz, *p*-cym); 2.54 (*dsept*, $J = 6.9$, 7.0 Hz, C<u>H</u>$(CH_3)_2$-16); 2.13 (*s*, CH_3-13); 1.03 (*d*, $J = 7.0$ Hz, CH(C<u>H</u>$_3)_2$-16); 1.01 (*d*, $J = 6.9$ Hz, CH(C<u>H</u>$_3)_2$-16). ^{13}C NMR (CD_2Cl_2 125.75 MHz) ppm: 166.82 (C-6); 156.25 (C-5); 154.78 (C-1); 151.07 (C-7); 140.37 (C-3); 136.79 (C-10); 130.85 (C-4); 130.60 (C-9/C-11); 130.02 (C-2); 124.30 (C-8/C-12); 107.85, 104.63, 87.37, 86.57, 86.31 and 85.69 (C-13 to C-18 *p*-Cym); 31.77 (<u>C</u>H$(CH_3)_2$-16); 22.47 and 22.27 (CH(<u>C</u>$H_3)_2$-13/16); 19.12 (*p*-Cym <u>C</u>H_3). IV (KBr, cm^{-1}): 1617 ($\nu_{C=N}$ imine), 1562 ($\nu_{C=N}$ pyridine). UV/Vis (CH_3CN, 5×10^{-5} mol L^{-1}) λ/nm (log ε, L mol^{-1} cm^{-1}): 257 (4.14); 317 (4.08), 421 (3.61). CV (CH_3CN/HTBA 0.1 mol L^{-1}): $E_{ox} = 1.20$ V, $E_{red} = 1.15$ V, $E½ = 1.17$ V. Molar conductivity in CH_3CN (or CH_2Cl_2) (1.0×10^{-3} mol L^{-1}) Λm (ohm^{-1} cm^2 mol^{-1}): 79.53 (9.95).

[RuCl(*p*-cym)(Memp)]PF_6 (4)

Yellow powder, yield 85–90% (0.094 g). *Anal.* calc. for $C_{23}H_{26}ClN_2F_6PRu$ (%) (exp.): C 45.12 (45.40), H 4.28 (4.27), N 4.58 (4.58). ^{1}H NMR (CD_2Cl_2 500.13 MHz) ppm: 9.21 (*brd*, $J = 5.5$ Hz, H-1); 7.67–7.60 (*m*, H-2); 8.04–7.97 (*m*, H-3/H-4); 8.32 (*s*, H-6); 7.28 (*d*, $J = 7.9$ Hz, H-8/H-12); 7.52 (*d*, $J = 7.9$ Hz, H-9/H-11); 5.63 (*d*, $J = 6.2$ Hz, *p*-cym); 5.37 (*d*, $J = 6.2$ Hz, *p*-cym); 5.29 (*d*, $J = 6.1$ Hz, *p*-cym); 5.20 (*d*, $J = 6.1$ Hz, *p*-cym); 2.54 (*dsept*, $J = 6.9$, 7.0 Hz, C<u>H</u>$(CH_3)_2$-16); 2.12 (*s*, CH_3-13); 0.99 (*d*, $J = 7.0$ Hz, CH(C<u>H</u>$_3)_2$-16); 0.97 (*d*, $J = 6.9$ Hz, CH(C<u>H</u>$_3)_2$-16). ^{13}C NMR ($CDCl_3$ 125.75 MHz) ppm: 165.31 (C-6); 156.26 (C-5); 154.90 (C-1); 150.23 (C-7); 141.72 (C-10); 140.25 (C-3); 130.89 (C-9/C-11); 130.27 (C-2); 129.70 (C-4); 122.60 (C-8/C-12); 107.50, 104.80; 87.37, 86.57, 86.31 and 85.69 (C-13 to C-18 *p*-Cym); 31.69 (<u>C</u>H$(CH_3)_2$-16); 22.41 and 22.25 (CH(<u>C</u>$H_3)_2$-13/16); 19.12 (*p*-Cym <u>C</u>H_3). IV (KBr, cm^{-1}): 1618 ($\nu_{C=N}$ imine), 1560 ($\nu_{C=N}$ pyridine). UV/Vis (CH_3CN, 5×10^{-5} mol L^{-1}) λ/nm (log ε, L mol^{-1} cm^{-1}): 257 (4.11); 317 (4.08), 423 (3.62). CV (CH_3CN/HTBA 0.1 mol L^{-1}): $E_{ox} = 1.17$ V, $E_{red} = 1.12$ V, $E½ = 1.14$ V. Molar conductivity in CH_3CN (or CH_2Cl_2) (1.0×10^{-3} mol L^{-1}) Λm (ohm^{-1} cm^2 mol^{-1}): 74.58 (13.91).

[RuCl(*p*-cym)(Tbump)]PF_6 (5)

Yellow powder, yield 85% (0.090). *Anal.* Calc. for $C_{26}H_{32}ClN_2F_6PRu$ (%): calc. (exp.) C 47.75 (47.64), H 4.93 (4.77), N 4.28 (4.68). ^{1}H NMR (CD_2Cl_2 500.13 MHz) ppm: 9.23 (*brd*, $J = 5.5$ Hz, H-1); 7.68–7.62 (*m*, H-2); 8.04–7.99 (*m*, H-3/H-4); 8.34 (*s*, H-6); 7.59 (*d*, $J = 8.1$ Hz, H-8/H-12); 7.51 (*d*, $J = 8.1$ Hz, H-9/H-11); 5.66 (*d*, $J = 6.2$ Hz, *p*-cym); 5.39 (*d*, $J = 6.2$ Hz, *p*-cym); 5.33 (*d*, $J = 6.1$ Hz, *p*-cym); 5.23 (*d*, $J = 6.1$ Hz, *p*-cym); 2.54 (*dsept*, $J = 6.9$, 7.0 Hz, C<u>H</u>$(CH_3)_2$-16); 2.14 (*s*, CH_3-13); 1.31 (*s*, ^{t}Bu C(<u>C</u>$H_3)_3$); 1.00 (*d*, $J = 7.0$ Hz, CH(C<u>H</u>$_3)_2$-16); 0.99 (*d*, $J = 6.9$ Hz, CH(C<u>H</u>$_3)_2$-16). ^{13}C NMR ($CDCl_3$ 125.75 MHz) ppm: 165.31 (C-6); 156.26 (C-5); 154.90 (C-1); 150.23 (C-7); 140.25 (C-3); 130.89 (C-9/C-11); 130.85 (C-10); 130.27 (C-2); 129.70 (C-4); 122.60 (C-8/C-12); 107.50, 104.80; 87.37, 86.57, 86.31 and 85.69 (C-13 to C-18 *p*-Cym); 31.69 (<u>C</u>H$(CH_3)_2$-16); 22.44 and 22.24 (CH(<u>C</u>$H_3)_2$-13/16); 19.12 (*p*-Cym <u>C</u>H_3); 31.79 (^{t}Bu <u>C</u>$(CH_3)_3$); 22.24 (^{t}Bu C(<u>C</u>$H_3)_3$). IV (KBr, cm^{-1}): 1617 ($\nu_{C=N}$ imine), 1562 ($\nu_{C=N}$ pyridine). UV/Vis (CH_3CN, 5×10^{-5} mol L^{-1}) λ/nm (log ε, L mol^{-1} cm^{-1}): 259 (4.08); 329 (4.03), 420 (3.61). CV (CH_3CN/HTBA 0.1 mol L^{-1}): $E_{ox} = 1.18$ V, $E_{red} = 1.15$ V, $E½ = 1.16$ V. Molar conductivity in CH_3CN (or CH_2Cl_2) (1.0×10^{-3} mol L^{-1}) Λm (ohm^{-1} cm^2 mol^{-1}): 75.29 (12.54).

[RuCl(*p*-cym)(Diemp)]PF_6 (6)

Orange powder, yield 90% (0.096 g). *Anal.* Calc. for

$C_{26}H_{32}ClN_2F_6PRu$ (%): calc. (exp.) C 47.75 (48.13), H 4.93 (5.01), N 4.28 (4.33). ^{1}H NMR (CD_2Cl_2 500.13 MHz) ppm: 9.36 (*brs*, H-1); 8.37 (*s*, H-6); 8.08 (*brd*, $J = 7.3$ Hz, H-3); 8.01 (*brd*, $J = 7.9$ Hz, H-4); 7.76 (*brs*, H-2); 7.36 (*brt*, $J = 7.2$, H-10); 7.31 (*d*, $J = 7.2$ Hz, H-9); 7.25 (*brd*, $J = 7.2$ Hz, H-11); 5.42 (*brs*, *p*-cym); 5.34 (*brd*, $J = 6.2$ Hz, *p*-cym); 5.29 (*brs*, *p*-cym); 5.08 (*brs*, *p*-cym); 3.10–2.98 (*m*, C<u>H</u>$(CH_3)_2$-12); 2.72–2.61 (*m*, C<u>H</u>$(CH_3)_2$-8); 2.61–2.54 (*m*, C<u>H</u>$(CH_3)_2$-16); 2.54–2.43 (*m*, CH($\underline{CH_3}$)$_2$-12); 2.33–2.21 (*m*, CH($\underline{CH_3}$)$_2$-8); 2.08 (*s*, CH_3-13); 1.06 (*brs*, CH($\underline{CH_3}$)$_2$-16); 1.22 (*brs*, CH($\underline{CH_3}$)$_2$-12); 0.98 (*brs*, CH($\underline{CH_3}$)$_2$-8). ^{13}C NMR ($CDCl_3$ 125.75 MHz) ppm: 170.81 (C-6); 156.65 (C-5); 154.32 (C-1); 150.11 (C-7); 140.49 (C-3); 138.10 (C-8); 134.77 (C-12); 130.45 (C-9); 130.22 (C-11); 130.00 (C-10); 128.29 (C-2); 127.61 (C-4); 109.40, 101.17; 88.58, 88.14, 85.96 and 85.78 (C-13 to C-18 *p*-Cym); 31.72 (C<u>H</u>$(CH_3)_2$-16); 26.18 and 24.92 (Diemp $\underline{C}H_2CH_3$); 22.54, 22.46 and 18.82 (*p*-Cym $\underline{C}H_3$); 16.26 and 15.76 (Diemp $-CH_2\underline{C}H_3$). IV (KBr, cm^{-1}): 1616 ($\nu_{C=N}$ imine), 1559 ($\nu_{C=N}$ pyridine). UV/Vis (CH_3CN, 5×10^{-5} mol L^{-1}) λ/nm (log ε, L mol^{-1} cm^{-1}): 264 (4.11); 364 (3.65), 427 (3.51). CV (CH_3CN/HTBA 0.1 mol L^{-1}): $E_{ox} = 1.21$ V, $E_{red} = 1.16$ V, $E^{1}/_{2} = 1{,}18$ V. Molar conductivity in CH_3CN (or CH_2Cl_2) (1.0×10^{-3} mol L^{-1}) Λm (ohm^{-1} cm^2 mol^{-1}): 78.92 (16.33).

[RuCl(*p*-cym)(Di*i*pmp)]PF_6 (7)

Yellow powder, yield 95% (0.105 g). *Anal.* Calc. for $C_{27}H_{36}ClN_2F_6PRu$ (%): calc. (exp.) C 49.31 (49.14), H 5.32 (5.38), N 4.11 (4.01). ^{1}H NMR (CD_2Cl_2 500.13 MHz) ppm: 9.36 (*brd*, $J = 5.5$ Hz, H-1); 8.28 (*s*, H-6); 8.11 (*ddd*, $J = 7.9$, 7.6, 1.1 Hz, H-3); 8.03 (*brd*, $J = 7.9$ Hz, H-4); 7.80 (*ddd*, $J = 7.6$, 5.5, 1.6 Hz, H-2); 7.44 (*brt*, $J = 8.0$, H-10); 7.36 (*d*, $J = 8.0$ Hz, H-9); 7.35 (*d*, $J = 8.4$ Hz, H-11); 5.62 (*d*, $J = 6.2$ Hz, *p*-cym); 5.47 (*d*, $J = 6.2$ Hz, *p*-cym); 5.33 (*d*, $J = 6.1$ Hz, *p*-cym); 5.05 (*d*, $J = 6.1$ Hz, *p*-cym); 3.69 (*sep*, $J = 6.8$ Hz, C<u>H</u>$(CH_3)_2$-12); 2.66 (*sep*, $J = 6.7$ Hz, C<u>H</u>$(CH_3)_2$-8); 2.54 (*dsept*, $J = 6.9$, 7.0 Hz, C<u>H</u>$(CH_3)_2$-16); 2.15 (*s*, CH_3-13); 1.43 (*d*, $J = 6.8$ Hz, CH($\underline{CH_3}$)$_2$-12); 1.26 (*d*, $J = 6.8$ Hz, CH($\underline{CH_3}$)$_2$-12); 1.13 (*d*, $J = 6.7$ Hz, CH($\underline{CH_3}$)$_2$-8); 0.84 (*d*, $J = 6.7$ Hz, CH($\underline{CH_3}$)$_2$-8). ^{13}C NMR ($CDCl_3$ 125.75 MHz) ppm: 170.97 (C-6); 156.87 (C-5); 154.18 (C-1); 148.84 (C-7); 142.52 (C-12); 140.55 (C-8); 139.90 (C-3); 130.54 (C-10); 130.31 (C-9); 130.23 (C-11); 125.63 (C-2); 125.22 (C-4); 108.46, 102.31; 88.32, 87.21, 86.36 and 85.28 (C-13 to C-18 *p*-Cym); 31.65 (C<u>H</u>$(CH_3)_2$-16); 28.75, 28.47, 27.56 and 26.27 (Di*i*pmp C($\underline{C}H_3)_2$); 24.00 (Di*i*pmp $\underline{C}(CH_3)_2$); 22.98, 22.39 and 18.97 (*p*-Cym $\underline{C}H_3$). IV (KBr, cm^{-1}): 1615 ($\nu_{C=N}$ imine), 1563 ($\nu_{C=N}$ pyridine). UV/Vis vis (CH_3CN, 5×10^{-5} mol L^{-1}) λ/nm (log ε, L mol^{-1} cm^{-1}): 266 (4.08), 368 (3.51), 428 (3.58). CV (CH_3CN/HTBA 0.1 mol L^{-1}): $E_{ox} = 1.20$ V, $E_{red} = 1.16$ V, $E^{1}/_{2} = 1.18$ V. Molar conductivity in CH_3CN (or CH_2Cl_2) (1.0×10^{-3} mol L^{-1}) Λm (ohm^{-1} cm^2 mol^{-1}): 71.72 (16.88).

[RuCl(*p*-cym)(O–O′)] (8)

Deprotonation of 2-hydroxyacetophenone (HAP, 40 μL; 0.33 mmol) was carried out in a Schlenk tube (100 mL) with a solution of methanol (5 mL) containing NaOH (14.6 mg; 3.6 mmol) under Ar atmosphere. After 1 h of reaction, the binuclear complex [RuCl(μ-Cl)(*p*-cym)]$_2$ (0.1 g; 0.16 mmol) was added and the reaction was magnetically stirred for 24 h at 60 °C. Then, the solvent removed under reduced pressure and the solid residue was dissolved in CH_2Cl_2 (3.0 mL), passed through a celite pad in order to remove NaCl. The filtered was collected in a Schlenk flask (100 mL) and addition of hexane (10 mL) yielded a brown solid. The solid was separated by filtration, washed with hexane (3×5 mL) and dried under reduced pressure.

Brown powder, yield 95% (124.76 mg). *Anal.* Calc. for $C_{18}H_{21}ClO_2Ru$ (%): calc. (exp.) C 53.27 (53.38), H 5.21 (5.29). ^{1}H NMR ($CDCl_3$ 500.13 MHz) ppm: 7.36 (*d*, $J_{HH} = 8.0$ Hz, 1H 2-acetylbenzenolate); 7.17 (*t*, $J_{HH} = 8.0$ Hz, 1H 2-acetylbenzenolate); 6.77 (*d*, $J_{HH} = 8.0$ Hz, 1H, 2-acetylbenzenolate); 6.36 (*t*, $J_{HH} = 8.0$ Hz, 1H 2-acetylbenzenolate); 5.21 (*dd*, $J_{HH} = 5.9$ Hz, 2H *p*-cym.) 2.89 (*sept*. $J_{HH} = 6.9$ Hz, *p*-cym.); 2.51 (*s*, CH_3, 2-acetylbenzenolate); 2.22 (*s*, CH_3, *p*-cym.); 1.32 (*d*, $J_{HH} = 6.9$ Hz, 6H *p*-cym.). ^{13}C NMR ($CDCl_3$ 125,75 MHz) ppm: 198.53 (C-7); 170.34 (C-1); 137.14 (C-3); 133.15 (C-5); 125.08 (C-6); 120.58 (C-4); 114.72 (C-2); 100.36, 97.82, 83.47, 82.81, 79.73, 79.41 (*p*-Cym. arom.); 31.49 (*p*-Cym. $\underline{C}H(CH_3)_2$.); 27.19 (2-acetylbenzenolate $\underline{C}H_3$); 22.72, 22.62 and 18.23 (*p*-Cym $\underline{C}H_3$). IV (KBr, cm^{-1}): 1587 ($\nu_{C=O}$).

2.4. Catalytic experiments

A standard procedure for reduction of aryl ketones is described as follow: In a Schlenk flask, the ketone (acetophenone or 4-methylacetophenone) (10 mmol) was dissolved in 2-propanol (2 mL) and refluxed at 82 °C within 5 min under inert Ar atmosphere. In a separate flask, the ruthenium complex (10 μmol) was dissolved in degassed 2-propanol (3 mL) in the presence of 1 mL of KOH (0.2 mol L^{-1} in 2-propanol), and then, the resulting suspension was transferred via cannula to the reaction flask and refluxed for 1 h at 82 °C. After that, an aliquot (1.0 mL) was withdrawn and diluted to 10 mL with an acid solution of 2-propanol (10 μL HCl; 11.0 mmol L^{-1}). Conversions were determined by gas chromatography using hexadecane as an internal standard (1.46 μL; 0.1 mmol L^{-1}). [Ru]/substrate/KOH = 1/1000/20.

2.5. Kinetic experiments

The kinetic studies of the transfer-hydrogenation of acetophenone were carried out in a stainless-steel autoclave Parr – Model 4842 with a volume capacity of 100 cm^3 equipped with an overhead magnetic stirrer, a digital pressure indicator and a thermocouple to record temperature. The autoclave was equipped with an electrical heating/cooling system to control the temperature inside the vessel. In a typical reaction, the catalyst precursor (ruthenium complexes **(3)** and **(7)**, (10 μmol) was dissolved in 2-propanol (58 mL) inside the autoclave in the presence 1 mL of KOH (0.2 mol L^{-1} in 2-propanol) and acetophenone (10 mmol) under Ar atmosphere ([Ru]/substrate/KOH = 1/1000/20). After that, the autoclave was repeatedly flushed with H_2 (3 times), and then the autoclave was pressurized with H_2 (10 bar). The autoclave was heated to the desired temperature (60–80 °C), and stirring at 450 rpm, for 120 min. The time-dependent analysis of the catalyzed reduction of acetophenone to 1-phenylethanol was performed after withdrawing aliquots (1.0 mL) every 5 min, for 20 min, and then every 10 min until the final time (120 min). Each aliquot was diluted to 10 mL with an acid solution of 2-propanol (10 μL HCl; 11.0 mmol L^{-1}) in the presence of hexadecane (1.46 μL; 0.1 mmol L^{-1}) and analyzed by gas chromatography (GC – FID).

2.6. X-ray diffraction data

The single-crystals were mounted on a goniometer in a Bruker KAPPA APEX II DUO diffractometer using graphite-monochromated MoKα ($\lambda = 0.71073$ Å) radiation. The final unit cell parameters were based on all reflections. Data were collected with the BRUKER APEX2 software package, with integration and scaling of the reflections performed using the BRUKER SAINT program [32,33]. Absorption correction was carried out by the multiscan method

Table 1
Crystal data and structure refinement of the [RuCl(*p*-cym)(Memp)PF_6 (**4**), [RuCl(*p*-cym)(Di*i*pmp)PF_6 **(7)** and [RuCl(*p*-cym)(O–O′)] (**8**).

	[RuCl(*p*-cym)(Memp)PF_6	[RuCl(*p*-cym)(Di*i*pmp)PF_6	[RuCl(*p*-cym)(O–O′)]
Empirical formula	$C_{23}H_{26}ClF_6N_2PRu$	$C_{28}H_{36}ClF_6N_2PRu$	$C_{18}H_{21}ClO_2Ru$
Formula weight	611.95	682.08	405.87
Temperature (K)	296(2)	296(2)	296(2)
Wavelength Å	0.71073	0.71073	0.71073
Crystal system	Monoclinic	Monoclinic	Triclinic
Space group	$P2_1/c$	$P2_1/n$	P-1
Unit cell dimensions			
a(Å)	9.0203(11)	17.5444(8)	7.6484(2)
b(Å)	26.272(3)	10.2274(5)	9.4401(3)
c(Å)	11.2706(14)	17.7350(8)	12.7883(4)
α(°)	90	90	72.8300(10)
β(°)	109.913(4)	108.997(2)	80.4030(10)
γ(°)	90	90	80.1890(10)
V(Å^3)	2511.2(5)	3008.9(2)	862.61(4)
Z	4	4	2
Density (calculated) (Mg/m^3)	1.619	1.506	1.563
Absorption coefficient (mm^{-1})	0.853	0.721	1.067
F(000)	1232	1392	412
Crystal size (mm^3)	0.380 × 0.280 x 0.270	0.250 × 0.100 x 0.040	0.250 × 0.160 x 0.070
Theta range for data collection (°)	2.072 to 26.538	1.988 to 26.412	1.680 to 26.448
Index ranges	$-11 \le h \le 11$ $-32 \le k \le 32$ $-14 \le l \le 14$	$-21 \le h \le 21$ $-12 \le k \le 12$ $-22 \le l \le 22$	$-9 \le h \le 9$ $-11 \le k \le 11$ $-15 \le l \le 15$
Reflections collected	35254	46914	11623
Independent reflections	5189[R(int) = 0.0431]	6168 [R(int) = 0.0453]	3542 [R(int) = 0.0208]
Completeness to theta maximum (%)	25.242°, 99.9%	25.242°, 100.0%	25.24°, 100%
Absorption correction [40]	Semi-empirical from equivalents	Semi-empirical from equivalents	Semi-empirical from equivalents
Refinement method	Full-matrix least-squares on F^2	Full-matrix least-squares on F^2	Full-matrix least-squares on F^2
Data/restraints/parameters	5189/0/311	6168/54/390	3542/0/203
Goodness-of-fit on F^2	1.212	1.042	1.058
Final R indices [$I > 2\sigma(I)$]	$R_1 = 0.0597$ $wR_2 = 0.1382$	$R_1 = 0.0504$, $wR_2 = 0.1287$	$R_1 = 0.0233$ $wR_2 = 0.0580$
R indices (all data)	$R_1 = 0.0653$ $wR_2 = 0.1417$	$R_1 = 0.0670$, $wR_2 = 0.1429$	$R_1 = 0.0267$ $wR_2 = 0.0604$
Largest diff. peak and hole (e. Å^{-3})	1.037 and −1.038	1.804 and −3.397	0.441 and −0.257

[33]. The structures were solved by direct methods with SHELXS-97 and models were refined by full-matrix least-squares on F^2 with SHELXL-2016 [34]. All hydrogen atoms were stereochemically positioned and refined applying the riding model [34]. The MERCURY views were prepared with Mercury 3.10.3 [35]. Table 1 summarizes the data collection and experimental details for [RuCl(*p*-cym)(Memp)PF_6 (**4**), [RuCl(*p*-cym)(Di*i*pmp)]PF_6 **(7)** and [RuCl(*p*-cym)(O–O′)] **(8)**.

2.7. Theoretical calculations

All structures were optimized with the Density Functional Theory (DFT) method based on the M06 functional [36]. The basis set employed was the Los Alamos effective core potential and double-zeta valence basis set (LanL2DZ) [37] for ruthenium and 6-31G(d) [38] for the remaining atoms. The solvation with acetonitrile was simulated with the use of the integral equation formalism variant of Polarizable Continuum Model (IEF-PCM). The absorption spectra were obtained with TD-DFT formalism and the above mentioned functional and basis set. All calculations were carried out using the software Gaussian 09 [39].

3. Results and discussion

3.1. Syntheses and structural characterization

The half-sandwich ruthenium (II) complexes with N–N′–pyridylimine ligands were obtained from the well-known binuclear complexes described by Bennett and Smith [41], [RuCl(μ-Cl)(*p*-cym)]$_2$. The two chlorido bridges between the metal centers in **(1)** were broken in the presence of these chelating ligands, in methanol solution containing PF_6^- salt, producing two equivalents of an orange – yellow mononuclear complexes with general formula [RuCl(*p*-cym)(N–N′)](PF_6). The elemental analyses (%C, %H, %N) agree with the proposed formulation for the complexes **(2)** to **(7)** and the molar conductivities were measured in CH_2Cl_2 or CH_3CN solutions, and are in the accepted range for 1:1 electrolytes. Scheme 1 contains the general structure and numbering of the half-sandwich ruthenium complexes reported here. All complexes are air stable and soluble in polar solvents such as dichloromethane, acetone or acetonitrile, and insoluble in apolar solvents, such as hexane or diethyl ether.

The infrared spectra of the complexes **(2)**–**(7)** confirmed the coordination of the ligands to the ruthenium center (Table 2). The $\nu_{C=Nimine}$ stretching frequencies are shifted from the range 1642–1626 cm^{-1} for the free ligands to 1618–1615 cm^{-1} after coordination. These shifts are due to the electron withdrawing nature of the ligands, which allows the M→L back-bonding interaction causing the weakening of the C=N bond and the $\nu_{C=Nimine}$ is shifted to lower wavenumbers. The $\nu_{C=Npyridine}$ is also shifted to lower wavenumbers, from the range 1568–1562 cm^{-1} to 1559–1563 cm^{-1}. The intensity of the bands for the metal complexes is also lower than for the free ligands, which indicates the loss of degrees of freedom upon coordination of the N–N' pyridylimine ligands to the ruthenium center. This behavior may also be attributed to the change of symmetry between the species. In addition, the presence of ν_{PF6-} counter-ion was confirmed by the occurrence of an intense band around 841–835 cm^{-1}.

The coordination of the N– N′–pyridylimine ligands was also confirmed by ^{1}H and ^{13}C NMR spectra, by comparing the spectra of the free ligands and the complexes **(2)**–**(7)**. The ^{1}H NMR spectra show a doublet signal for the pyridine hydrogen in the range 9.21–9.36 ppm (See the ^{1}H and ^{13}C NMR spectra in the supplementary material), which is shifted when compared to the same

Table 2
Selected IR stretching frequencies, and ^{1}H and ^{13}C NMR chemical shifts of the pyridylimine ligands and complexes **(2)**–**(7)**.

Free ligand	Complex	IR stretching (cm^{-1})		^{1}H NMR (ppm)		^{13}C NMR (ppm)
		$\nu_{C=N\ imine}$	$\nu_{C=N\ pyridine}$	$HC{=}N_{imine}$	$HC{=}N_{pyridine}$	$HC{=}N_{imine}$
Amp		1633	1568	8.45	8.50	161.47
	(2)	1618	1559	8.37	9.24	166.16
Clmp		1626	1565	8.43	8.53	160.84
	(3)	1617	1562	8.38	9.22	166.82
Memp		1627	1565	8.39	8.46	159.52
	(4)	1618	1560	8.32	9.21	165.31
Tbump		1627	1566	8.49	8.53	160.67
	(5)	1617	1562	8.34	9.23	165.31
Diemp		1642	1565	8.21	8.58	164.04
	(6)	1616	1559	8.37	9.36	170.81
Di*i*pmp		1633	1568	8.31	8.73	162.97
	(7)	1615	1563	8.28	9.36	170.97

hydrogen signal in the free ligand. These signals are shifted to higher frequencies, due to the deshielding of the α-hydrogen of pyridine (H-1) owing to the coordination to the metal center (Table 2). Additionally, is also observed in the ^{1}H NMR spectra, a singlet signal in the range 8.28–8.38 ppm corresponding to the hydrogen nucleus attributed to the azomethine group (HC=N; H-6). In general, they were shielded when compared to the hydrogen of the azomethine group in the free ligands (8.21–8.49 ppm). The coordination of imine nitrogen weakens the C=N bond, thereby shielding the hydrogen of the azomethine group (see H-6 in the ^{1}H NMR spectra in the supplementary material). These results confirm the coordination of the N–N′–pyridylimine ligands to the ruthenium center, which agree with the infrared data.

It is known that the aromatic ^{1}H nuclei signals for the coordinated arene are found in the range 4–6 ppm [43]. However, the coordination of the N–N′–pyridylimine ligand to the ruthenium center provides a loss of the two-fold symmetry of the *p*-cymene arene. As a consequence, it is observed an arrangement of four doublets in the region 5.30–6.00 ppm for the aromatic hydrogen nuclei of the *p*-cymene. Additionally, the lower symmetry of the complexes is confirmed by the ^{1}H NMR spectrum of **(7)** (Fig. S11), in which three septet signals attributed to the isopropyl hydrogen (H-8, H-12 and H-16) of the *p*-cymene and N–N′–pyridylimine ligands are observed. This behavior has also been observed for similar ruthenium (II) complexes previously reported [25].

The ^{13}C NMR spectra of complexes **(2)**–**(7)** showed that coordination also affects the chemical shift of methine group of imine ligands observed in the range 159.52–164.04 ppm, for the free ligand, while for the complexes the range is shifted to 165.31–170.97 ppm (Table 2).

The X-ray structure of **(4)** has a ruthenium center coordinated to the N-(4-methylphenyl)-1-(pyridin-2-yl)methanimine (Memp), to a Cl atom and to the *p*-cymene aromatic ring, resulting in a piano-stool geometry (Fig. 1). The restricted bite angle of the Memp, N(1)–Ru–N(2) angle = 76.40° (17) supported the distorted structure and the torsion angle C6–N2–C7–C12 (125.8° (6)) supported the two planes described by the pyridine and the substituted phenyl ring. As a result, the substituted phenyl ring is almost coplanar to the *p*-cymene ring, while the pyridine ring is inclined relative to the position of the phenyl ring.

The chloride atom is on the same side of the methyl group of the *p*-cymene ligand. This behavior is also observed in related complexes previously described in the literature [25].

Complex **(7)** has crystallized in the monoclinic crystal system and $P2_1/c$ space group, which contains the N-[2,6-bis(propan-2-yl) phenyl]-1-(pyridin-2-yl)methanimine (Di*i*pmp), was previously reported by Friedrich et al. [25] Here, the structure was found to

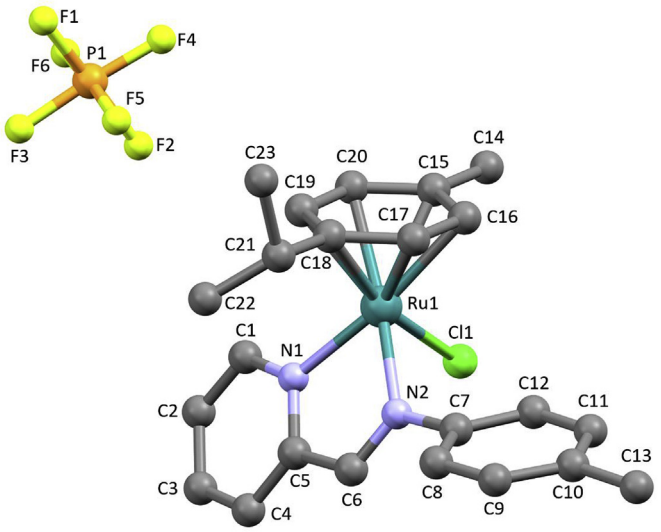

Fig. 1. MERCURY view and atomic labelling of $[RuCl(p\text{-cym})(Memp)]PF_6$ **(4).** The hydrogens were omitted for clarify. Bond Lengths (A): C(15)–Ru 2.242(6); C(16)–Ru 2.199(5); C(17)–Ru 2.166(5); C(18)–Ru 2.219(5); C(19)–Ru 2.168(5); C(20)–Ru 2.201(5), N(1)–Ru 2.088(4); N(2)–Ru 2.104(4); Cl(1)–Ru 2.3848(14). Bond Angles (°):Cl(1)–Ru–N(1) 83.60(12); Cl(1)–Ru–N(2) 85.40(12); Cl(1)–Ru–C(15) 87.79(16); Cl(1)–Ru–C(16) 98.44(17); Cl(1)–Ru–C(17) 130.79(17); Cl(1)–Ru–C(18) 167.04(17); Cl(1)–Ru–C(19) 141.35(16); Cl(1)–Ru–C(20) 105.79(16); N(1)–Ru–N(2) 76.40(17); N(1)–Ru–C(15) 135.3(2); N(2)–Ru–C(20) 168.81(19); N(1)–Ru–C(16) 171.8(2); N(1)–Ru–C(17) 143.8(2); N(1)–Ru–C(18) 108.9(2); N(1)–Ru–C(19) 93.50(19); N(1)–Ru–C(20) 104.6(2); N(2)–Ru–C(15) 146.5(2); N(2)–Ru–C(16) 111.6(2); N(2)–Ru–C(17) 93.37(19); N(2)–Ru–C(18) 100.60(19); N(2)–Ru–C(19) 131.47(19).

belong to the $P2_{1/n}$ space group, with a lower value of β angle. In both structures, the classical piano-stool geometry is also observed, with the chlorido ligand oriented to the same side of the methyl group of the *p*-cymene ligand. The pyridyl ring of the Di*i*pmp has an inclined angle much more apparent with respect to the imine ring than the Memp coordinated to the ruthenium center (See Fig. 2). Herein, the X-ray structure of **(7)** has a torsion angle C6–N2–⊖ C7–C12 of the 82.5° (5), while in the structure previously described by Friedrich et al. [25] the torsion angle is slightly larger (94.30°).

3.2. Electronic spectroscopy

The UV/Vis spectrum of the $[RuCl(\mu\text{-}Cl)(p\text{-cym})]_2$ presents two bands at $\lambda = 421$ and 327 nm, in acetonitrile solution (5.0×10^{-5} mol L^{-1}), with $\varepsilon = 1174$ and 1819 cm^{-1} L mol^{-1}. After coordination of the N–N′–pyridylimine ligands to the ruthenium center three bands region are observed in the spectra (Fig. 3A).

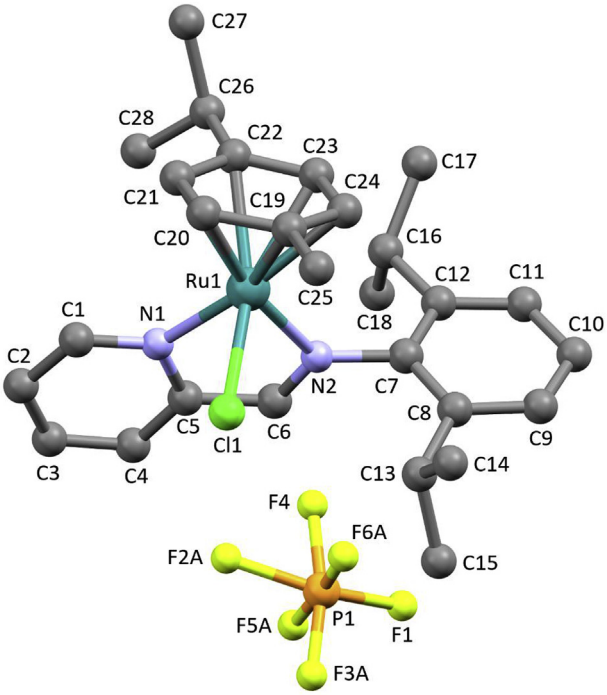

Fig. 2. MERCURY view and atomic labeling of [RuCl(*p*-cym)(Di*i*pmp)]PF_6 **(7)**. The hydrogens were omitted for clarify. Bond Lengths (A): C(19)–Ru 2.234(5); C(20)–Ru 2.196(5); C(21)–Ru 2.195(4); C(22)–Ru 2.239(4); C(23)–Ru 2.180(4); C(24)–Ru 2.201(5); N(1)–Ru 2.088(4); N(2)–Ru 2.115(3); Cl(1)–Ru 2.3852(11). Bond Angles (°):Cl(1)–Ru–N(1) 80.43(11); Cl(1)–Ru–N(2) 89.67(9); Cl(1)–Ru–C(23) 149.78(15); Cl(1)–Ru–C(21) 119.89(15); Cl(1)–Ru–C(20) 91.37(14); Cl(1)–Ru–C(24) 112.18(15); Cl(1)–Ru–C(19) 87.96(14); Cl(1)–Ru–C(22) 157.12(13); N(1)–Ru–N(2) 76.68(13); N(1)–Ru–C(23) 129.61(18); N(1)–Ru–N(2) 76.68(13).

The region 1 with λ value around 260 nm has a hyperchromic effect in the presence of the N–N′–pyridylimine ligands, mainly with the N-(2,6-diethylphenyl)-1-(pyridin-2-yl)methanimine (Diemp) and N-[2,6-bis(propan-2-yl)phenyl]-1-(pyridin-2-yl) methanimine (Di*i*pmp).

The complexes **(2)**, **(3)**, **(4)** and **(5)**, in which the *p*-substituents of the phenyl are –H, $-CH_3$, –*t*-But and –Cl show an increasing of the absorbance band around 310–330 nm (ε between 8912 and 10471 $cm^{-1}\,L\,mol^{-1}$), which were designed as region 2. However, the complexes **(6)** and **(7)** (Diethyl or di*iso*propyl *ortho*-substitutes) do not have this band resolved. Indeed, this band has low intensity, λ values at 364 and 368 nm, with $\varepsilon = 4365$ and 3801 $cm^{-1}\,L\,mol^{-1}$, respectively, and a bathochromic shift compared to the other complexes.

The region 3 around $\lambda = 420$ nm (with ε in the range 3235 and 4073 $cm^{-1}\,L\,mol^{-1}$) remains virtually the same for all complexes, as observed for the precursor [RuCl(μ-Cl)(*p*-cym)]$_2$.

In order to better understand the transition involved in the regions 1, 2 and 3 a M06/TD-DFT calculation was carried out to generate a theoretical electronic spectrum of the regions for each complex. The calculated and experimental spectra have good correlation, as can be observed in Fig. 3A and B.

Complexes **(2)** and **(7)** were selected to illustrate the results in the TD-DFT calculation. The composition of the orbitals involved in the transition in the region 2 for **(2)** and regions 1, 2 and 3 for **(7)** in the UV/Vis spectrum are depicted in Table 3. The molecular orbitals in the region 2 for both complexes are displayed in Fig. 4. The results in all regions for the complexes **(2)**–**(7)** are available in the supplementary material (Figures S15 - S20 and Schemes S1 – S.16).

In the region 3 of the UV/Vis spectra, the complexes **(2)**–**(7)** present a mixed contribution of both Ru and Cl to G_1 and G_2, explaining the slightly variation of the absorbance bands in this region. These bands were attributed to metal to ligand charge transfer (MLCT), HOMO-1 → LUMO and HOMO-1 → LUMO+1, as can be seen in Table 3 for the complex **(7)**.

In the region 2 of the TD-DFT calculated spectrum (Fig. 3B), the complex **(2)** presents a band at 341 nm. The excited state related to this transition presents two dominant electronic configurations, related to HOMO-3 → LUMO and HOMO-2 → LUMO transitions, which are basically MLCT Ru → G_2, as can be seen in Fig. 4. The complexes **(3)**, **(4)** and **(5)** (Fig. 3, Schemes S4 – S.6 and Fig. S16 – S18) have the same behavior as observed for **(2)** in the region 2 of the UV/Vis spectra. These facts lead to the conclusion that the *p*-substituent groups of the imino ring (–H, $-CH_3$, –*t*-But and –Cl) do

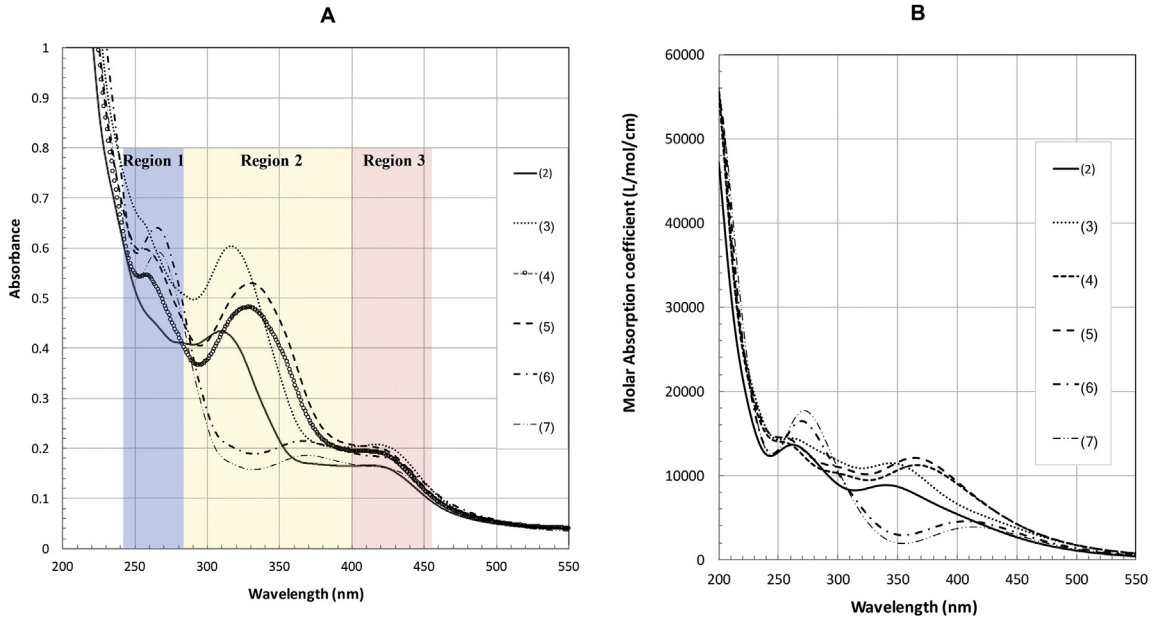

Fig. 3. A) UV/Vis spectra of the complexes from **(2)** to **(7)** in acetonitrile solution (5.0×10^{-5} mol L^{-1}. B) Theoretical electronic spectra for the related complexes.

Table 3
Composition of some selected molecular orbitals of **(2)** and **(7)**.

Complex	$\lambda_{Calc.}$ (nm)	$\lambda_{Exp.}$ (nm)	Main Transitions	MOs	% of contributions						
					Ru	Cl	R^1	$R^{1'}$	R^2	G_1	G_2
(2) Region 2	341	318	HOMO-3→LUMO	LUMO	5	2	0	0	0	3	90
			HOMO-2→LUMO	HOMO-3	23	8	0	0	0	8	61
				HOMO-2	46	13	0	0	0	7	34
(7) Region 3	411	428	HOMO-1→LUMO	LUMO+1	52	11	0	0	0	22	15
			HOMO-1→LUMO+1	LUMO	8	4	0	0	0	4	84
				HOMO-1	59	22	0	0	0	9	10
(7) Region 2	367	368	HOMO-2→LUMO	LUMO	8	4	0	0	0	4	84
			HOMO-3→LUMO	HOMO-2	1	0	5	6	0	0	87
			HOMO-4→LUMO	HOMO-3	35	5	1	1	0	5	53
				HOMO-4	43	10	1	2	0	10	34
(7) Region 1	268	267	HOMO-7→LUMO	LUMO+5	14	0	0	0	0	78	8
			HOMO-4→LUMO+4	LUMO+4	14	2	0	0	0	82	2
			HOMO-3→LUMO+4	LUMO+3	4	0	0	0	0	3	93
			HOMO-1→LUMO+3	LUMO	8	4	0	0	0	4	84
			HOMO-1→LUMO+4	HOMO-1	59	22	0	0	0	9	10
			HOMO-1→LUMO+5	HOMO-3	35	5	1	1	0	5	53
				HOMO-4	43	10	1	2	0	10	34
				HOMO-7	4	2	1	4	0	6	84

R^1 and $R^{1'}$ = *ortho* − substitution in the imino ring; R^2 = *para* − substitution in the imino ring; G_1 = *p*-cymene ligand and G_2 = N–N′ pyridyl − imine ligands.

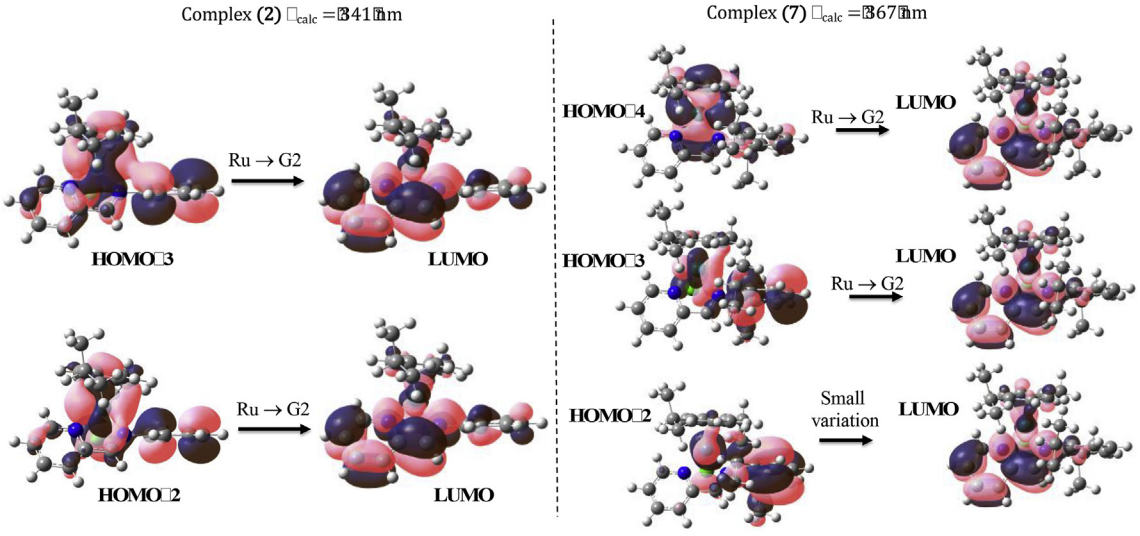

Fig. 4. Contour plots of some selected MOs of **(2)** and **(7)** in region 2 in the UV/Vis spectra.

not have a significantly interference in the transitions in the region 2.

The complex **(7)** in the TD-DFT calculated spectrum presents a transition at 367 nm, matching well with the experimental data observed at 368 nm. This excited state presents a multi-configurational character, involving transitions from HOMO-4, HOMO-3 and HOMO-2 transitions to LUMO, (Fig. 4). The HOMO-4 and HOMO-3 to LUMO relates to MLCT, specifically from Ru to N–N′–pyridylimine ligand (G_2). The HOMO-2 to LUMO relates to an internal transition located at G_2. This transition has a small oscillator strength (f = 0.0049) and this weak transition is also observed for complex **(6)**, in agreement with the experimental spectra (figures S19 – S.20 and Schemes S7 – S.8).

Additionally, in the region 1, complex **(6)** presents one intense transition at 267 nm and complex **(7)** presents two transitions at 268 and 270 nm. The excited states related to these transitions present high multi-configurational character, being in general dominated by Ru → G_1 and Ru → G_2.

3.3. Electrochemical characterization

The electrochemical behavior of **(2)** – **(7)** was investigated by cyclic voltammetry, recorded at glassy carbon as working electrode in TBAH (0.10 mol L^{-1}) acetonitrile solutions. All complexes present one irreversible anodic process (E_{pa}) at 1.8 V, and a reversible redox process with half-wave potential ($E^{1}/_{2}$) in the region 1.14–1.18 V, which are dependent of the E_{pa} at 1.8 V. A representative voltammogram for the complexes is depicted in Fig. 5A for **(7)**.

The E_{pa} at 1.8 V is attributed to Ru^{II} → Ru^{III} process with simultaneous displacement of the *p*-cymene ring. As a result a solvento complex with general formula $[Ru^{3+}Cl(N{-}N)(CH_3CN)_3]^{2+}$ is formed in the presence of acetonitrile as solvent, which is reduced to $[Ru^{2+}Cl(N{-}N)(CH_3CN)_3]^{+}$ at around 1.09 V. The electrochemical behavior is depicted in Scheme 2 showing the species observed in the cyclic voltammograms for the complexes **(2)**–**(7)**.

An electrolysis at constant potential (1.85 V) was carried out for complex **(7)**, and within 1 h an increasing of the current of the reversible process around $E^{1}/_{2}$ at 1.18 V and concomitant decreasing

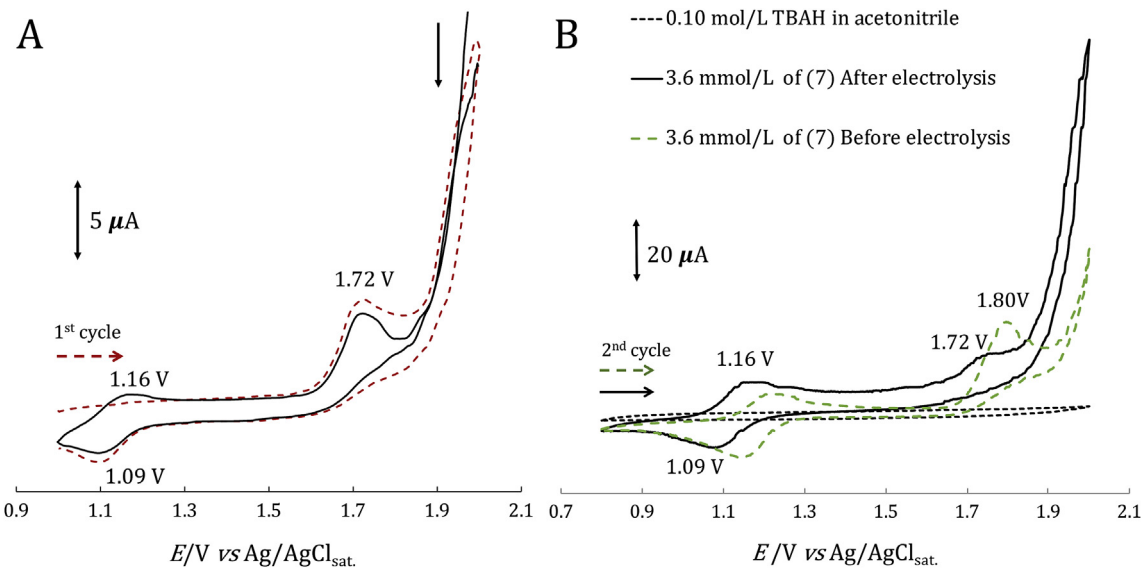

Fig. 5. A) CV of the complex **(7)** with one cycle anodic and cathodic. B) CV of the complex **(7)** (2nd cycle) after and before electrolysis at 1.85 V. The cyclic voltammograms (CV) were recorded using glassy carbon as working electrode in acetonitrile solution of TBAH 0.10 mol L^{-1} at sweep rate of 100 mV s^{-1}.

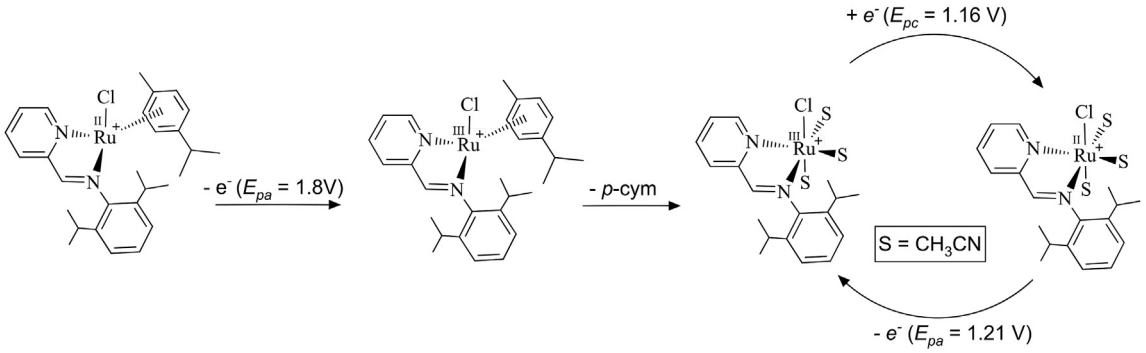

Scheme 2. Proposed mechanism for the cyclic voltammetry behavior of the complexes, exemplified for **(7)** [42].

of the irreversible process at 1.8 V was observed (Fig. 5B). The electrolysis also reveals a great increasing of the current at 2.0 V, assumed to be the oxidation process of the free *p*-cymene. In order to corroborate to the result described, it was previously described that the oxidation of limonene, which is structurally similar to the *p*-cymene, has an oxidation process at 1.89 V, in the same conditions of the experiments performed here [44].

As expected the displacement of N–N′–pyridylimine ligand by the acetonitrile after oxidation to form $[Ru^{3+}Cl(p\text{-cym})(CH_3CN)_2]^{2+}$ was ruled out, once the electrochemical process for this complex occurs at $E½ = 1.31$ V. The cyclic voltammogram of $[RuCl(p\text{-cym})(CH_3CN)_2]^{+}$, which was obtained by independent synthesis according to procedure described by Sadler and coworkers, is presented in Fig. S21 [45]. Additionally, the electrochemical behavior of the free ligand Diipmp presents two anodic processes centered at 1.48 and 1.90 V (Fig. S22), which have no similarity with the cyclic voltammetric behavior of the complexes **(2)**–**(7)**. Table 4 summarizes the electrochemical data for the half-sandwich ruthenium complex presented in this work.

Table 4
Cyclic voltammetry data for the complexes **(2)**–**(7)**.

Complex	E_{pa} (V) $Ru^{II} \rightarrow Ru^{III}$	E_{pa} (V)	E_{pc} (V)	$E½$ (V)
(2)	1.77	1.18	1.14	1.16
(3)	1.77	1.22	1.15	1.19
(4)	1.75	1.19	1.12	1.16
(5)	1.76	1.21	1.14	1.18
(6)	1.78	1.22	1.16	1.19
(7)	1.78	1.22	1.16	1.19

E_{pa} = anodic potential peak; E_{pc} = cathodic potential peak; $E½$ = half-wave potential = $(E_{pa} + E_{pc})/2$.

3.4. Catalysis

The transfer-hydrogenation reactions of the acetophenone and 4- methylacetophenone catalyzed by complexes **(2)**–**(7)** were performed using isopropanol as H_2-source and KOH as co-catalyst, at 82 °C. The conversions (%) are the average of three independent reactions carried out in the same conditions, Table 5.

Reactions were carried out in isopropanol (5.0 mL), in the presence of KOH (1.0 mL, 0.1 mol L^{-1} in isopropanol), aryl ketone (10 mmol), and pre-catalyst (10 μmol) at 82 °C within 3 h [Ru]/substrate/KOH molar ratio = 1/1000/20. [a]Substrate: acetophenone or 4-methylacetophenone. [b]Hydrogenated products were determined by gas chromatography using *n*-hexadecane as internal standard. [c]*Sd* = standard deviation. TON = *turnover number* = mol of product/mol of pre-catalyst. TOF = *turnover frequency* = mol of product/mol of pre-catalyst/time.

Table 5
Transfer hydrogenation of acetophenone and 4-methylacetophenone catalyzed by complexes **(2)**–**(7)**.

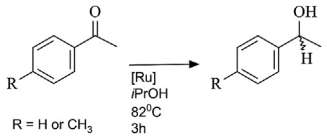

Complexes	Acetophenone[a]			4-methylacetophenone[a]		
	TON	TOF (h^{-1})	% Product[b] ± *Sd*[c]	TON	TOF (h^{-1})	% Product[b] ± *Sd*[c]
(2)	899	300	90.0 ± 7.0	697	232	69.8 ± 11.0
(3)	818	272	81.8 ± 1.5	819	273	82.0 ± 2.0
(4)	906	302	90.5 ± 6.0	841	280	84.2 ± 2.8
(5)	872	291	87.2 ± 10.7	253	84	25.3 ± 1.6
(6)	639	213	63.9 ± 4.5	755	252	75.5 ± 9.1
(7)	633	211	63.3 ± 3.8	856	232	85.6 ± 3.6

All complexes showed good catalytic activity for the transfer hydrogenation of acetophenone, but complexes **(2)** and **(4)** presented the best results with productivity up to 90.0% and 90.5% of 1-phenylethanol, respectively. The rates of 300 and 291 h^{-1} for **(2)** and **(4)**, respectively, were obtained within 3 h of reaction. The conversion values point out to the dependence of the pre-catalyst performance on the nature of the N–N′–pyridylimine ligand.

The results presented in Table 5, similarly show conversion of 63.9% and 63.3% of 1-phenylethanol when the complexes **(6)** and **(7)** were used as pre-catalysts. Since the electrochemical processes and electronic spectroscopy of these complexes are very close to each other (Table 4), it is fair enough to assume that the electronic effect of the substituents does not play a significant role in the catalytic performance of **(6)** and **(7)**. Therefore, the decrease in the amount of the hydrogenated product when **(6)** and **(7)** was used as pre-catalysts is attributed to the steric hindrance caused by the substituents in the positions 2 and 6 of the imino ring (See Scheme 1).

The percentage of 1-phenylethanol produced was very close when the complexes **(3)** and **(5)** were used as pre-catalyst, 81.8% and 87.2% respectively. However, the standard deviation for **(5)** was higher than the observed for the other complexes studied here for the transfer hydrogenation of acetophenone, providing a variation of ±10.7% in the amount of 1-phenylethanol.

All complexes also showed good catalytic productivity in the transfer hydrogenation of 4-methylphenylethanol, except complex **(5)**, which yielded only 25.3% of hydrogenated product with rate of 84 h^{-1}, after 3 h of reaction. This result suggests that the great steric hindrance of *tert*-butyl group substituted in the N–N′–pyridylimine ligand is playing a role. Additionally, the 4-methylacetophenone is more basic than the acetophenone, which decreases the electrophilicity of the carbon atom of the carbonyl group of the ketone. However, the amount of hydrogenated product increases when the substrate was changed from the acetophenone to 4-methylacetophenone in the presence of the complexes **(6)** and **(7)** as pre-catalysts. This remarkable result, suggests a better orientation of the 4-methylacetophenone to the metal center when **(6)** and **(7)** are used as pre-catalysts. Possibly, these complexes containing steric demanding ligands can modulate the strength of the bonding between the substrate and the metal center. Aiming the better understanding the catalytic transfer-hydrogenation of ketones discussed here, kinetic experiments in the temperature range of 60–80 °C were conducted using the complexes **(3)** and **(7)** as pre-catalysts, see the discussion presented in the next section.

When the catalyzed reaction in performed in absence of KOH reduction of the ketones was not observed, suggesting the formation of a ruthenium-alkoxide intermediate [46,47], which can produce a ruthenium hydride complex by β-hydride elimination. This ruthenium hydride complex is assumed as the catalyst of the transfer hydrogenation reaction, as described in Scheme 3.

Additionally, the 2-hydroxyacetophenone (HAP) was used as substrate in the transfer hydrogenation reaction, using the complexes **(2)**–**(7)** as pre-catalyst in the same conditions described to acetophenone and 4-methylacetophenone, but the pre-catalysts were inactive, and the corresponding alcohol was not observed. The basic medium of the reaction (KOH) suggests the deprotonation of the 2-hydroxyacetophenone, which could provide a chelating ligand to coordinate and generate a stable complex, poisoning the catalytic system. In order to verify this hypothesis, a reaction between $[RuCl(\mu\text{-}Cl)(p\text{-cym})]_2$ **(1)** and HAP in the presence of NaOH in methanol solution was carried out at 60 °C within 24 h of reaction. A brown powder was isolated in 95% yield, which was characterized as a neutral mononuclear complex with general formula $[RuCl(p\text{-cym})(O\text{–}O')]$ **(8)** {where O–O′ = 2-acetylbenzenolate}. Elemental analysis (C, H) agrees with the proposed formulation for **(8)**, as well as the ^{1}H and ^{13}C NMR data reinforce the molecular structure determined by X-ray diffraction (Fig. 6).

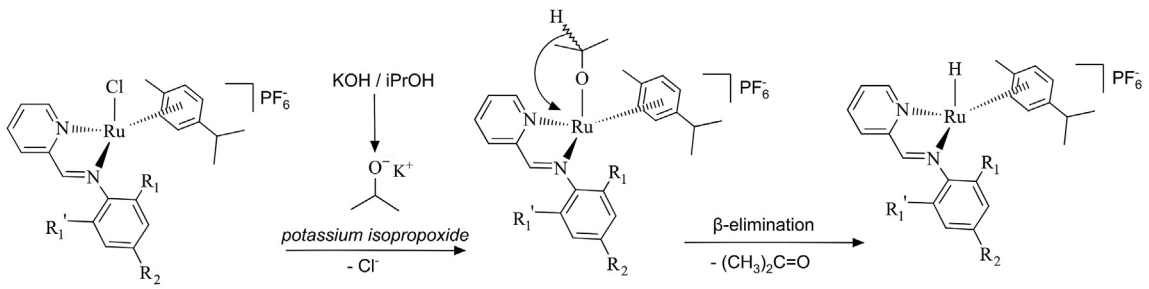

Scheme 3. Suggestion for ruthenium hydride complexes formed in situ for complexes **(2)**–**(7)** [42].

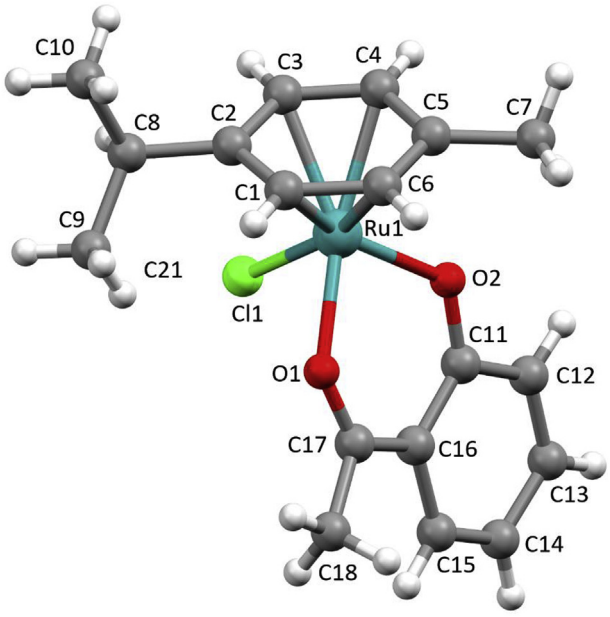

Fig. 6. MERCURY view and atomic labelling of [RuCl(*p*-cym)(O-O′)] **(8)** showing the atom labelling and 50% probability ellipsoids. Bond Lengths (A): C(1)–Ru(1) 2.160(2); C(2)–Ru(1) 2.191(2); C(3)–Ru(1) 2.152(2); C(4)–Ru(1) 2.168(2); C(5)–Ru(1) 2.180(2); C(6)–Ru(1) 2.170(2); O(1)–Ru(1) 2.0805(14); O(2)–Ru(1) 2.0473(16); Cl(1)–Ru(1) 2.4240(6); C(11)–O(2) 1.302(3); C(17)–O(1) 1.248(3). Bond Angles (°): C(1)-C(2)-Ru(1) 69.99(13); C(3)-C(2)-Ru(1) 69.31(13), C(4)-C(3)-Ru(1) 71.80(13); C(2)-C(3)-Ru(1) 72.30(12); C(3)-C(4)-Ru(1) 70.56(12); C(5)-C(4)-Ru(1) 71.41(13); C(6)-C(5)-Ru(1) 70.69(13); C(4)-C(5)-Ru(1) 70.50(13); C(1)-C(6)-Ru(1) 70.60(12); O(2)-Ru(1)-O(1) 85.82(6); O(2)-Ru(1)-Cl(1) 85.96(5); O(1)-Ru(1)-Cl(1) 85.21(5).

The X-ray structure of **(8)** has a ruthenium center coordinated to the 2-acetylbenzenolate (O–O′), the chlorido and the *p*-cymene ring, resulting in a neutral piano-stool structure (Fig. 6). The restricted bite angle of the O–O′, O(2)-Ru(1)-O(1) = 85.82° (6), supported the distorted structure with planes described by the 2-acetylbenzenolate and *p*-cymene ring. Unlike the other structures presented in this work, the chlorido ligand is on the opposite side of the methyl group of the *p*-cymene ring, demonstrating the coordination capacity of the *p*-cymene ring to favor different relative orientations of the ligands around the ruthenium center. This structure agrees with other enolate-containing ruthenium complexes reported elsewhere [48–53].

3.5. Kinetic study

The complexes [RuCl(*p*-cym)(Clmp)]PF_6 **(3)** and [RuCl(*p*-cym)(-Di*i*pmp)]PF_6 **(7)** were chosen for the kinetic studies of the transfer hydrogenation reaction of acetophenone, due to their steric hindrance and electronic effect in the *ortho* and *para* – positions of the imino ring in the N–N′–pyridylimine ligands, respectively. The kinetic experiments were carried out in a stainless-steel autoclave using the same molar ratio [Ru]/substrate/KOH = 1/1000/20, described in the last section, but in the presence of 10 bar of H_2, in the temperature range of 60–80 °C.

The conversion *vs*. time plots for **(3)** and **(7)** for each temperature studied are presented in Fig. 7. The curves have a sigmoidal shape for both, with an induction time of ~20 min. The activity of the complex **(3)** is significantly more sensible to the temperature variation than the complex **(7)**. The final conversion for **(7)** is less affected by the temperature than complex **(3)**, with an average of 65% yield of 1-phenylethanol, within 2 h of reaction. This result is very close to that obtained in the absence of H_2 within 3 h of reaction (Table 5). However, the productivity of the complex **(3)** was more affected, increasing the temperature from 60 °C to 80 °C the yield of 1-phenylethanol increases from only 8%–86%. This result was also close to that obtained without H_2 pressure within 3 h of reaction.

For the first order conditions, the rate constant *k* was increased with the increasing of temperature when the hydrogenation reaction of acetophenone was catalyzed by **(3)** and **(7)** (see Table 6 and Fig. 8), but in the presence of **(3)**, the change was much more pronounced; e.g. at 80 °C the *k* value was 18-fold higher than at

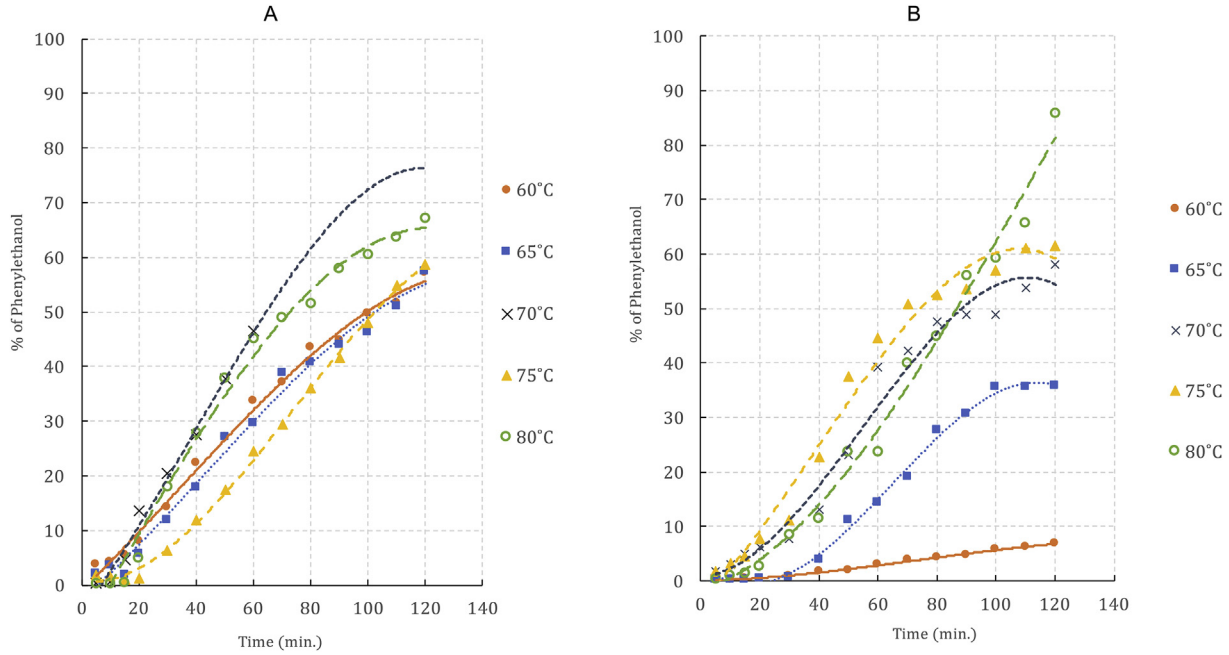

Fig. 7. Plots of % of 1-phenylethanol versus time for hydrogenation of acetophenone at temperature range 60–80 °C. A) For [RuCl(*p*-cym)(Di*i*pmp)]PF_6 **(7)** as pre-catalyst. B) For [RuCl(*p*-cym)(Clmp)]PF_6 **(3)** as pre-catalyst.

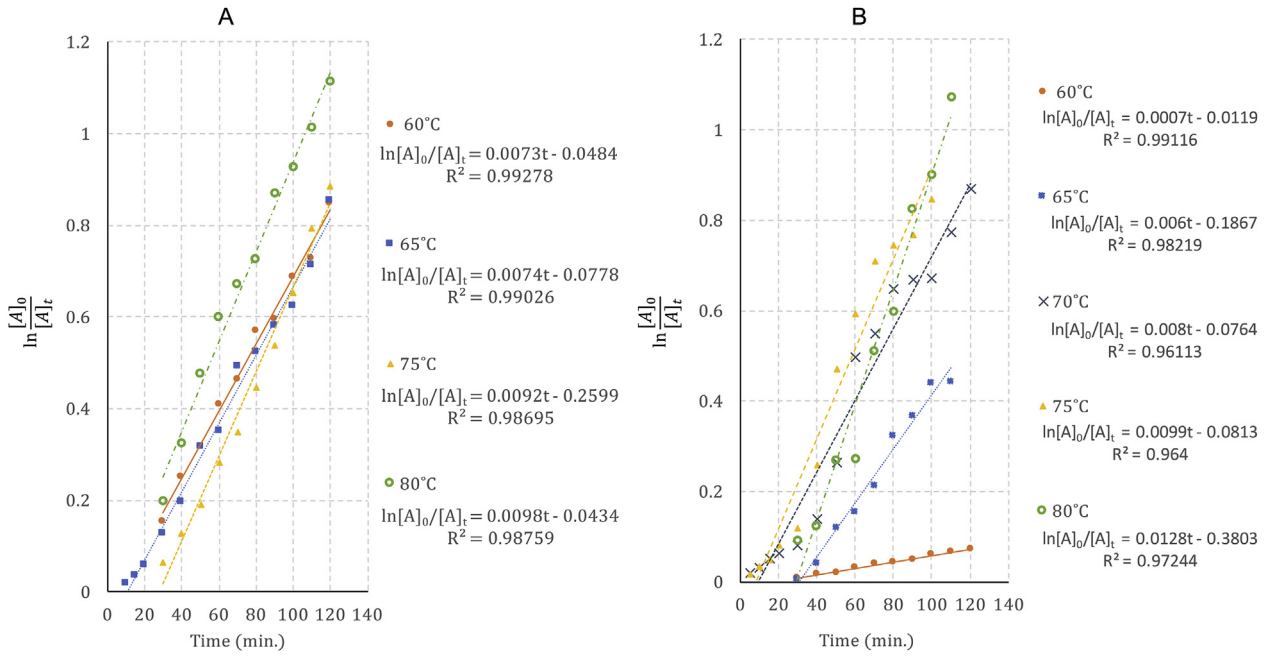

Fig. 8. Plots of ln $[A]_0/[A]t$ versus time for hydrogenation of acetophenone at temperature range 60–80 °C. Using as pre-catalyst, A) [RuCl(*p*-cym)(Diipmp)]PF_6 **(7),** and B) [RuCl(*p*-cym)(Clmp)]PF_6 **(3)**.

Table 6
Kinetics parameters for hydrogenation of acetophenone, using [RuCl(*p*-cym)(Clmp)]PF_6 **(3)** and [RuCl(*p*-cym)(Diipmp)]PF_6 **(7)** as pre-catalysts under first order conditions.

Temperature (°C)	[RuCl(*p*-cym)(Diipmp)](PF_6)		[RuCl(*p*-cym)(Clmp)](PF_6)	
	k (min.$^{-1}$) × 10^{-3}	$t_{1/2}$ (min.)	k (min.$^{-1}$) × 10^{-3}	$t_{1/2}$ (min.)
60	7.3	95	0.7	990
65	7.4	94	6.0	116
70	–	–	8.0	87
75	9.2	75	9.9	70
80	9.8	71	12.8	54

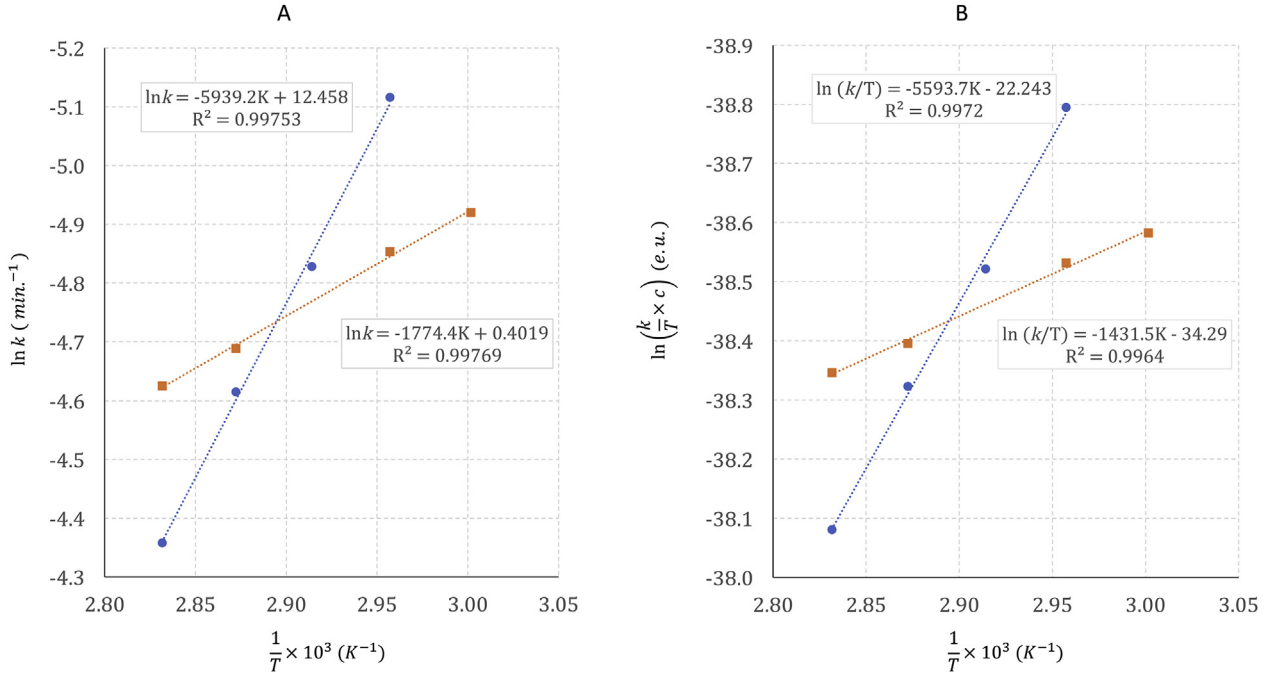

Fig. 9. A) An Arrhenius plot for hydrogenation of acetophenone. B) An Eyring plot for hydrogenation of acetophenone. Blue circle = [RuCl(*p*-cym)(Clmp)]PF_6 **(3)**, and orange square = [RuCl(*p*-cym)(Diipmp)]PF_6 **(7)**. (For interpretation of the references to color in this figure legend, the reader is referred to the Web version of this article.)

Table 7
Thermodynamic activation parameters for hydrogenation of acetophenone using [RuCl(*p*-cym)(Clmp)]PF_6 **(3)** and [RuCl(*p*-cym)(Di*i*pmp)]PF_6 **(7)** as pre-catalysts.

Complex	*A*	E^a(kJ mol^{-1})	$\Delta H^{\neq}$ (kJ mol^{-1})	$\Delta S^{\neq}$ *e.u.*[a] (J mol^{-1} K^{-1})
(3)	257300.52	49.38	46.51	−22.24 (−184.90)
(7)	1.49	14.75	11.90	−34.29 (−285.09)

[a] *e.u.* = energy unity for $\Delta S^{\#}/R$ values.

60 °C, and $t_{½}$ was decreased from 990 min to 54 min. As expected, in the presence of complex **(7)**, the rate constant was less affected, suggesting different activation parameters for these complexes. Therefore, an Arrhenius and an Eyring plots, Fig. 9A and B respectively, were constructed in order to obtain the thermodynamic activation parameters (Table 7).

Half-life. $t_{1/2} = \frac{ln2}{k}$

A plot of ln(k) versus (1/T) gives a straight line with slope $-E_a/R$ and intercept ln (A), where R is the gas constant = 8.314 J mol^{-1} K^{-1} (Fig. 9A). The data in Table 7 shows that the activation energy (E_a) was 3-fold lower for **(3)** when compared with **(7)**, and the pre-exponential factors (A) are very different. These results suggest a small activation barrier between the acetophenone and transition state (the highest energy point) for a reaction profile comparing the complex **(3)** and **(7)** as pre-catalyst.

The Eyring plot, $ln\left(\frac{k}{T} \times c\right)$ versus $\frac{1}{T}$ {where k = rate constant; T = absolute temperature and $c = 7.99 \times 10^{-13}$ min^{-1} K^{-1} = $\frac{h}{\kappa'}$; {h = Planck's constant and κ' = Bolzman's constant} gives a straight line with slope $-\Delta H^{\neq}/R$ and intercept $\Delta S^{\neq}/R$ [54]. The large negative $\Delta S^{\neq}/R$ values for **(3)** and **(7)** suggest an associative mechanism. Particularly for **(7)**, the values of $\Delta S^{\neq}/R$ is lower than **(3)** (−34.29 and −22.24 *e.u.* respectively), which is attributed to a more organized interaction of the acetophenone and the catalyst in the transition state for complex **(7)** than **(3)**, most likely due to the steric hindrance of the isopropyl groups *ortho*-substituted in the N−N′pyridylimine ligand. Possibly, due to the steric hindrance of the complex **(7)**, the approximation of acetophenone and coordination to the ruthenium may be prevented. In this way, comparing the E_a and $\Delta S^{\neq}/R$ for both complexes may be considered that complex **(3)** catalyze the reaction through an inner-sphere mechanism, while complex **(7)** could adopt an outer-sphere mechanism assisted by the solvent or H_2, as suggested by Sinopalnikova et al. [55].

4. Conclusions

Five electron-rich N−N′−pyridylimine ligands were synthesized by the condensation reaction between 2-piridinecarboxyaldhehyde and the substituted anilines, which were used as chelating ligands for the preparation of half-sandwich ruthenium complexes. The complexes **(2)** and **(7)** were fully characterized and their structures were determined by physicochemical techniques, including, elemental analysis, ^{1}H and ^{13}C NMR data, infrared spectroscopy and X-ray diffraction for **(4)** and **(7)**. Additionally, due to the lack of activity of the complexes to reduce the 2-hydroxyacetophenone, its reactivity with the dimer **(1)** was studied revealing the formation of a neutral half-sandwich congener ruthenium complex **(8)** and its the molecular structure are also presented and discussed. This lack of activity was rationalized in terms of reaction of the substrate shifting the pyridylimine ligands and resulting in a stable neutral complex, which is favored by the large excess of the substrate in the transfer hydrogenation conditions. The electrochemical behavior of the complexes **(2)**–**(7)** revealed an irreversible anodic process mainly centered on Ru^{2+} around 1.8 V. Coupled to this process, a reversible one appears around $E½ = 1.2$ V. The complexes **(2)**–**(8)** were applied as pre-catalyst in the transfer hydrogenation of the acetophenone and 4- methylacetophenone, showing good catalytic activity, with productivity up to 90% and rate of 300 h^{-1} within 3 h of reaction. A kinetic investigation using **(3)** and **(7)** as pre-catalysts showed that the time dependence for the production of 1-phenylethanol has a sigmoidal shape, with an induction time of ~20 min. The catalytic activity of **(3)** is more sensitive to the temperature variation, therefore, in this case, the rate constant (k) increases faster than for **(7)**. An Arrhenius plot suggests a smaller activation barrier between the acetophenone and transition state for complex **(7)** than for **(3)**, $E_a = 14.75$ and 49.38 kJ mol^{-1}, respectively. The $\Delta S^{\neq}/R$ values obtained from an Eyring plot shown values lower than − 10 *e.u.*, suggesting an associative transition state when these kinds of complexes are applied as pre-catalysts in the hydrogenation of acetophenone. Additionally, the differences in the electronic and steric properties of the complexes may suggest differences in the mechanism, which is supported by the activation parameters. For complex **(7)** a less energy demanding from the resting-state to transition state observed may be due to an outer-sphere mechanism assisted by the H_2-donor.

Notes

The authors declare no competing financial interest.

Acknowledgements

We thank FAPEMIG, CNPq, CAPES, FAPESP, FINEP, DAAD and RQ-MG for financial support. The authors are thankful to the Grupo de Materiais Inorgânicos do Triângulo (GMIT) research group supported by FAPEMIG.

Appendix A. Supplementary data

Supplementary data to this article can be found online at https://doi.org/10.1016/j.jorganchem.2019.04.022.

References

[1] R.H. Crabtree, The Organometallic Chemistry of the Transition Metals, fourth ed., John Wiley & Sons, Inc., New Jersey, 2005.
[2] C. Elschenbroich, Organometallics, third ed., WILEY-VCH Verlag, Weinheim, 2006.
[3] D. Steinborn, Fundamentals of Organometallic Catalysis, first ed., WILEY-VCH Verlag, Weinheim, 2012.
[4] M. Cotton, F. Albert, Geoffrey Wilkinson, Carlos A. Murillo, Bochmann, Advanced Inorganic Chemistry, sixth ed., John Wiley & Sons, New York, 1999.
[5] R. Noyori, H. Takaya, BINAP: an efficient chiral element for asymmetric catalysis, Acc. Chem. Res. 23 (1990) 345–350, https://doi.org/10.1021/ar00178a005.
[6] N. Ryoji, O. Takeshi, Asymmetric catalysis by architectural and functional molecular engineering: practical chemo- and stereoselective hydrogenation of ketones, Angew. Chem. Int. Ed. 40 (2001) 40–73, https://doi.org/10.1002/1521-3773(20010105)40:1<40::AID-ANIE40>3.0.CO;2-5.
[7] R.D. Nascimento, A.K. Silva, L.M. Lião, V.M. Deflon, L.T. Ueno, L.R. Dinelli, A.L. Bogado, Mixed diphosphine/diamine ruthenium (II) isomers: synthesis, structural characterization and catalytic hydrogenation of ketones, J. Mol. Struct. 1151 (2018) 277–285, https://doi.org/10.1016/j.molstruc.2017.09.044.
[8] D.A. Cavarzan, F.D. Fagundes, O. Fuganti, C.W.P. Da Silva, C.B. Pinheiro, D.F. Back, A. Barison, A.L. Bogado, M.P. De Araujo, Mixed phosphine/diimines and/or amines ruthenium carbonyl complexes: synthesis, characterization and transfer-hydrogenation, Polyhedron 62 (2013) 75–82, https://doi.org/10.1016/j.poly.2013.06.022.
[9] T.F. Gallatti, A.L. Bogado, G. Von Poelhsitz, J. Ellena, E.E. Castellano, A.A. Batista, M.P. de Araujo, Heterobimetallic [Ru(II)/Fe(II)] complexes: on the formation of trans- and cis-[RuCl2(dppf)(diimines)], J. Organomet. Chem. 692 (2007) 5447–5452, https://doi.org/10.1016/j.jorganchem.2007.08.038.
[10] L. Bogado, G. Von Poelhsitz, J. Ellena, E.E. Castellano, C.L. Donnici, V. Comasseto, A. a Batista, Ruthenium Phosphine/Diimine Complexes : Syntheses , Characterization , Reactivity with Carbon Monoxide , and Catalytic Hydrogenation of Ketones, 2005, pp. 6159–6168.

[11] L.C.M. Souza, T.A. Santos, C.R.A. Do Prado, B.A.V. Lima, R.S. Corrêa, A.A. Batista, L. Otubo, J. Ellena, L.T. Ueno, L.R. Dinelli, A.L. Bogado, Influence of gold nanoparticles applied to catalytic hydrogenation of acetophenone with cationic complexes containing ruthenium, RSC Adv. 6 (2016) 53130–53139, https://doi.org/10.1039/c6ra05616d.

[12] S. Denizalti, D. Mercan, B. Şen, A.G. Gökçe, B. Çetinkaya, Asymmetric transfer hydrogenation reaction in water: comparison of chiral proline amide/amine ruthenium(II) complexes, J. Organomet. Chem. 779 (2015) 62–66, https://doi.org/10.1016/j.jorganchem.2014.12.023.

[13] D. Pandiarajan, R. Ramesh, Ruthenium(II) half-sandwich complexes containing thioamides: synthesis, structures and catalytic transfer hydrogenation of ketones, J. Organomet. Chem. 723 (2013) 26–35, https://doi.org/10.1016/j.jorganchem.2012.10.003.

[14] S. Dayan, N.K. Ozpozan, N. Özdemir, O. Dayan, Synthesis of some ruthenium(II)-Schiff base complexes bearing sulfonamide fragment: new catalysts for transfer hydrogenation of ketones, J. Organomet. Chem. 770 (2014) 21–28, https://doi.org/10.1016/j.jorganchem.2014.08.002.

[15] S. Kaufhold, L. Petermann, R. Staehle, S. Rau, Transition metal complexes with N-heterocyclic carbene ligands: from organometallic hydrogenation reactions toward water splitting, Coord. Chem. Rev. 304–305 (2015) 73–87, https://doi.org/10.1016/j.ccr.2014.12.004.

[16] X.H. Zhu, L.H. Cai, C.X. Wang, Y.N. Wang, X.Q. Guo, X.F. Hou, Efficient and versatile transfer hydrogenation catalysts: iridium (III) and ruthenium (II) complexes with 4-acetylbenzyl-N-heterocyclic carbenes, J. Mol. Catal. A Chem. 393 (2014) 134–141, https://doi.org/10.1016/j.molcata.2014.06.004.

[17] S. Yaşar, E.Ö. Karaca, Ç. Şahin, I. Özdemir, O. Şahin, O. Büyükgüngör, Novel ruthenium(II)-N-heterocyclic carbene complexes; Synthesis, characterization and catalytic application, J. Organomet. Chem. 789–790 (2015) 1–7, https://doi.org/10.1016/j.jorganchem.2015.04.012.

[18] A. Aktaş, Y. Gök, 4-Vinylbenzyl-substituted silver(I) N-heterocyclic carbene complexes and ruthenium(II) N-heterocyclic carbene complexes: synthesis and transfer hydrogenation of ketones, Transit. Met. Chem. 39 (2014) 925–931, https://doi.org/10.1007/s11243-014-9877-y.

[19] J. Volbeda, P.G. Jones, M. Tamm, Preparation of chiral imidazolin-2-imine ligands and their application in ruthenium-catalyzed transfer hydrogenation, Inorg. Chim. Acta 422 (2014) 158–166, https://doi.org/10.1016/j.ica.2014.06.026.

[20] M. Aydemir, K. Rafikova, N. Kystaubayeva, S. Paşa, N. Meriç, Y.S. Ocak, A. Zazybin, H. Temel, N. Gürbüz, I. Özdemir, Ionic liquid based Ru(II)-phosphinite compounds and their catalytic use in transfer hydrogenation: X-ray structure of an ionic compound 1-chloro-3-(3-methylimidazolidin-1-yl) propan-2-ol, Polyhedron 81 (2014) 245–255, https://doi.org/10.1016/j.poly.2014.05.079.

[21] J.M. Gichumbi, H.B. Friedrich, Half-sandwich complexes of platinum group metals (Ir, Rh, Ru and Os) and some recent biological and catalytic applications, J. Organomet. Chem. 866 (2018) 123–143, https://doi.org/10.1016/j.jorganchem.2018.04.021.

[22] J.M. Gichumbi, B. Omondi, G. Lazarus, M. Singh, N. Shaikh, H.Y. Chenia, H.B. Friedrich, Influence of halogen substitution in the ligand sphere on the antitumor and antibacterial activity of half-sandwich ruthenium(II) complexes [RuX(η6-arene)(C5H4N-2-CH=N-Ar)]+, Zeitschrift Fur Anorg. Und Allg. Chemie. 643 (2017) 699–711, https://doi.org/10.1002/zaac.201600427.

[23] J.M. Gichumbi, H.B. Friedrich, B. Omondi, Synthesis and characterization of piano-stool ruthenium complexes with N , N' -pyridine imine bidentate ligands and their application in styrene oxidation, J. Organomet. Chem. 808 (2016) 87–96, https://doi.org/10.1016/j.jorganchem.2016.02.015.

[24] J.M. Gichumbi, B. Omondi, H.B. Friedrich, Oxidation of olefins catalyzed by half-sandwich osmium(II) arene complexes, J. Organomet. Chem. 856 (2018) 56–62, https://doi.org/10.1016/j.jorganchem.2017.12.038.

[25] J.M. Gichumbi, H.B. Friedrich, B. Omondi, Inorganica Chimica Acta Synthesis and characterization of some new half-sandwich ruthenium (II) complexes with bidentate N , N 0 -ligands and their application in alcohol oxidation 456 (2017) 55–63.

[26] J.M. Gichumbi, H.B. Friedrich, B. Omondi, Application of arene ruthenium(II) complexes with pyridine-2-carboxaldimine ligands in the transfer hydrogenation of ketones, J. Mol. Catal. A Chem. 416 (2016) 29–38, https://doi.org/10.1016/j.molcata.2016.02.012.

[27] J.M. Gichumbi, H.B. Friedrich, B. Omondi, Synthesis and characterization of half-sandwich ruthenium(II) complexes with N-alkyl pyridyl-imine ligands and their application in transfer hydrogenation of ketones, Transit. Met. Chem. 41 (2016) 867–877, https://doi.org/10.1007/s11243-016-0089-5.

[28] J.M. Gichumbi, H.B. Friedrich, B. Omondi, Application of arene ruthenium(II) complexes with pyridine-2-carboxaldimine ligands in the transfer hydrogenation of ketones, J. Mol. Catal. A Chem. 416 (2016) 29–38. https://doi.org/10.1016/j.molcata.2016.02.012.

[29] J.M. Gichumbi, B. Omondi, H.B. Friedrich, Half-sandwich osmium(II) complexes with bidentate N,N-chelating ligands and their use in the transfer hydrogenation of ketones, Eur. J. Inorg. Chem. 2017 (2017) 915–924, https://doi.org/10.1002/ejic.201601249.

[30] A.P.G. Kieboom, Purification of Laboratory Chemicals, D.D. Perrin and W. L. F. Armarego, third ed., WILEY-VCH Verlag, 1988 https://doi.org/10.1002/recl.19881071209.

[31] S. Dehghanpour, N. Bouslimani, R. Welter, F. Mojahed, Synthesis, spectral characterization, properties and structures of copper(I) complexes containing novel bidentate iminopyridine ligands, Polyhedron 26 (2007) 154–162. https://doi.org/10.1016/j.poly.2006.08.011.

[32] Bruker Bruker, APEX2, Bruker AXS Inc., Madison, Wisconsin, USA., 2012.

[33] Bruker Bruker, SAINT, Bruker AXS Inc., Madison, Wisconsin, USA, 2012.

[34] G.M. Sheldrick, A short history of SHELX, Acta Crystallogr. A 64 (2008) 112–122, https://doi.org/10.1107/S0108767307043930.

[35] C.F. Macrae, P.R. Edgington, P. McCabe, E. Pidcock, G.P. Shields, R. Taylor, M. Towler, J. Van De Streek, Mercury: visualization and analysis of crystal structures, J. Appl. Crystallogr. 39 (2006) 453–457, https://doi.org/10.1107/S002188980600731X.

[36] Y. Zhao, D.G. Truhlar, The M06 suite of density functionals for main group thermochemistry, thermochemical kinetics, noncovalent interactions, excited states, and transition elements: two new functionals and systematic testing of four M06-class functionals and 12 other function, Theor. Chem. Acc. 120 (2008) 215–241, https://doi.org/10.1007/s00214-007-0310-x.

[37] P.J. Hay, W.R. Wadt, Ab initio effective core potentials for molecular calculations. Potentials for the transition metal atoms Sc to Hg, J. Chem. Phys. 82 (1985) 270–283, https://doi.org/10.1063/1.448799.

[38] R. Ditchfield, W.J. Hehre, J.A. Pople, Self-consistent molecular-orbital methods. IX. An extended Gaussian-type basis for molecular-orbital studies of organic molecules, J. Chem. Phys. 54 (1971) 724–728, https://doi.org/10.1063/1.1674902.

[39] J.A, J.E.P, F.O, M.J.B, J.J.H, E.N.B, K.N.K, V.N.S, T.A.K, R.K, J.N, K.R, A.P.R, J.C.B, S.S.I, J.M.J. Frisch, G.W. Trucks, H.B. Schlegel, G.E. Scuseria, M.A. Robb, J.R. Cheeseman, G. Scalmani, V. Barone, G.A. Petersson, H. Nakatsuji, X. Li, M. Caricato, A.V. Marenich, J. Bloino, B.G. Janesko, R. G, Gaussian 09, Revision B.01, Gaussian 09, Revis. B.01, Gaussian, Inc., Wallingford CT, 2016.

[40] R.H. Blessing, An empirical correction for absorption anisotropy, Acta Crystallogr. A 51 (1995) 33–38, https://doi.org/10.1107/S0108767394005726.

[41] M.A. Bennett, A.K. Smith, Arene ruthenium(II) complexes formed by dehydrogenation of cyclohexadienes with ruthenium(III) trichloride, J. Chem. Soc., Dalton Trans. (1974) 233–241, https://doi.org/10.1039/DT9740000233.

[42] Marvin Was Used for Drawing and Displaying Chemical Structures and Reactions, chemAxon, Marvin 17.12.0, 2017. http://www.chemaxon.com.

[43] P.S. Pregosin, NMR in Organometallic Chemistry, first ed., WILEY-VCH Verlag, Weinheim, 2012.

[44] A.L. Bogado, R.F. De Souza, U. Schuchardt, A.A. Batista, On the kinetics of epoxidation of olefins by cis and trans-[RuCl2(dppb)(2,2′-bipy)] complexes, J. Mol. Catal. A Chem. 203 (2003) 129–135, https://doi.org/10.1016/S1381-1169(03)00353-4.

[45] A. Habtemariam, M. Melchart, R. Fernández, S. Parsons, I.D.H. Oswald, A. Parkin, F.P.A. Fabbiani, J.E. Davidson, A. Dawson, R.E. Aird, D.I. Jodrell, P.J. Sadler, Structure-activity relationships for cytotoxic ruthenium(II) arene complexes containing N,N-, N,O-, and O,O-chelating ligands, J. Med. Chem. 49 (2006) 6858–6868, https://doi.org/10.1021/jm060596m.

[46] W. Baratta, G. Chelucci, S. Gladiali, K. Siega, M. Toniutti, M. Zanette, E. Zangrando, P. Rigo, Ruthenium(II) terdentate CNN complexes: superlative catalysts for the hydrogen-transfer reduction of ketones by reversible insertion of a carbonyl group into the Ru-H bond, Angew. Chem. Int. Ed. 44 (2005) 6214–6219, https://doi.org/10.1002/anie.200502118.

[47] J. Halpern, B.R. James, Homogeneous catalysis of D2-H2O exchange by ruthenium-(III) chloride. Evidence for the heterolytic splitting of hydrogen, Can. J. Chem. 44 (1966) 671–675, https://doi.org/10.1139/v66-093.

[48] F. Basuli, A. Kumar Das, G. Mostafa, S.-M. Peng, S. Bhattacharya, Chemistry of ruthenium with some phenolic ligands: synthesis, structure and redox properties, Polyhedron 19 (2000) 1663–1672, https://doi.org/10.1016/S0277-5387(00)00404-6.

[49] S.L. Saraf, T.J. Fish, A.D. Benninghoff, A.A. Buelt, R.C. Smith, L.M. Berreau, Photochemical reactivity of Ru II (η 6 - p -cymene) flavonolato compounds, Organometallics 33 (2014) 6341–6351, https://doi.org/10.1021/om5006337.

[50] J. Kljun, A.K. Bytzek, W. Kandioller, C. Bartel, M.A. Jakupec, C.G. Hartinger, B.K. Keppler, I. Turel, Physicochemical studies and anticancer potency of ruthenium η6-p-cymene complexes containing antibacterial quinolones, Organometallics 30 (2011) 2506–2512, https://doi.org/10.1021/om101180c.

[51] D. Carmona, J. Ferrer, L.A. Oro, J. Elguero, M.L. Jimeno, c1– (1), (1990).

[52] F. Caruso, M. Rossi, A. Benson, C. Opazo, D. Freedman, E. Monti, M.B. Gariboldi, J. Shaulky, F. Marchetti, R. Pettinari, C. Pettinari, Ruthenium – arene complexes of curcumin: X-ray and density functional theory structure, synthesis, and spectroscopic characterization, in: In Vitro Antitumor Activity, and DNA Docking Studies of (P -Cymene)Ru(curcuminato)chloro, 2012.

[53] G.K. Lahiri, Ruthenium phenolates, Chemistry 82 (1988) 4396–4402.

[54] J.D. Atwood, Inorganic and Organometallic Reaction Mechanisms, second ed., WILEY-VCH Verlag, 1997.

[55] I.S. Sinopalnikova, T.A. Peganova, N.V. Belkova, E. Deydier, J.C. Daran, E.S. Shubina, A.M. Kalsin, R. Poli, Ruthenium p-cymene iminophosphonamide complexes: activation under basic conditions and transfer hydrogenation catalysis, Eur. J. Inorg. Chem. 2018 (2018) 2285–2299, https://doi.org/10.1002/ejic.201701344.